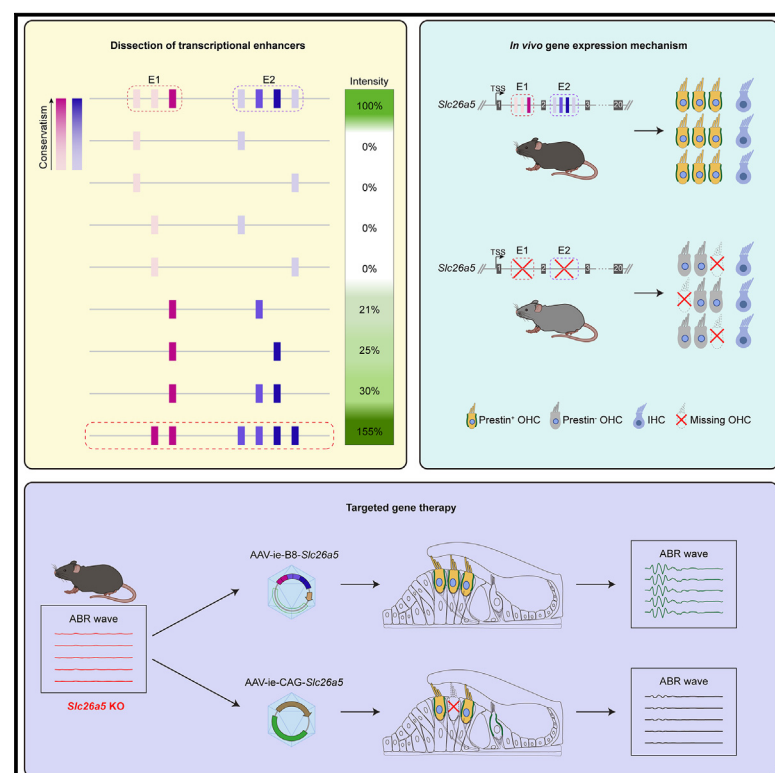# Deciphering enhancers of hearing loss genes for efficient and targeted gene therapy of hereditary deafness

Graphical abstract

Authors

Simeng Zhao, Qiuxiang Yang, Zehua Yu, ..., Chao-Po Lin, Yong-Gang Yao, Guisheng Zhong

Correspondence

zhaosm@shanghaitech.edu.cn (S.Z.), zhongsh@shanghaitech.edu.cn (G.Z.)

In brief

Zhao et al. establish an AAV-reporter-based *in vivo* transcriptional enhancer reconstruction (ARBITER) workflow to dissect enhancers of hearing loss genes. Using ARBITER, they decode the *Slc26a5* enhancers and engineer a highly efficient, outer hair cell (OHC)-specific enhancer. Gene therapy with this enhancer restores hearing function in *Slc26a5* KO mice.

Highlights

- ARBITER workflow allows reliable dissection of enhancers of hearing loss genes

- Two conserved non-coding elements (CNEs) regulate *Slc26a5* expression

- Engineering of a highly efficient and outer hair cell (OHC)-specific enhancer

- Targeted gene delivery restores auditory function of genetic hearing loss in mice

CellPress

Article

Deciphering enhancers of hearing loss genes for efficient and targeted gene therapy of hereditary deafness

Simeng Zhao,[1,9,*] Qiuxiang Yang,[1,2,9] Zehua Yu,[1,2,9] Cenfeng Chu,[1] Shengqi Dai,[1,2] Hongli Li,[3,6] Min Diao,[1] Lingyue Feng,[1,2] Junzi Ke,[1,2] Yilin Xue,[2] Qifang Zhou,[1,2] Yan Liu,[1] Hanhui Ma,[2] Chao-Po Lin,[2] Yong-Gang Yao,[3,6,7] and Guisheng Zhong[1,2,4,5,8,10,*]

[1]iHuman Institute, ShanghaiTech University, Shanghai 201210, China
[2]School of Life Science and Technology, ShanghaiTech University, Shanghai 201210, China
[3]State Key Laboratory of Genetic Evolution and Animal Models, Yunnan Key Laboratory of Animal Models and Human Disease Mechanisms, Yunnan Engineering Center on Brain Disease Models, KIZ-CUHK Joint Laboratory of Bioresources and Molecular Research in Common Diseases, Kunming Institute of Zoology, Chinese Academy of Sciences, Kunming, Yunnan 650204, China
[4]Shanghai Clinical Research and Trial Center, Shanghai 201210, China
[5]Shanghai Key Laboratory of High-Resolution Electron Microscopy, ShanghaiTech University, Shanghai 201210, China
[6]National Research Facility for Phenotypic & Genetic Analysis of Model Animals (Primate Facility), and National Resource Center for Non-Human Primates, Kunming Institute of Zoology, Chinese Academy of Sciences, Kunming 650107, Yunnan, China
[7]Kunming College of Life Science, University of Chinese Academy of Sciences, Kunming 650204, Yunnan, China
[8]Shanghai Key Laboratory of Gene Editing and Cell Therapy for Rare Diseases, Fudan University, Shanghai 20031, China
[9]These authors contributed equally
[10]Lead contact
*Correspondence: zhaosm@shanghaitech.edu.cn (S.Z.), zhongsh@shanghaitech.edu.cn (G.Z.)
https://doi.org/10.1016/j.neuron.2025.03.023

SUMMARY

Hereditary hearing loss accounts for about 60% of congenital deafness. Although adeno-associated virus (AAV)-mediated gene therapy shows substantial potential for treating genetic hearing impairments, there remain significant concerns regarding the specificity and safety of AAV vectors. The sophisticated nature of the cochlea further complicates the challenge of precisely targeting gene delivery. Here, we introduced an AAV-reporter-based *in vivo* transcriptional enhancer reconstruction (ARBITER) workflow, enabling efficient and reliable dissection of enhancers. With ARBITER, we successfully demonstrated that the conserved non-coding elements (CNEs) within the gene locus collaboratively regulate the expression of *Slc26a5*, which was further validated using knockout mouse models. We also assessed the potential of identified enhancers to treat hereditary hearing loss by conducting gene therapy in *Slc26a5* mutant mice. Based on the original *Slc26a5* enhancer with limited efficiency, we engineered a highly efficient and outer hair cell (OHC)-specific enhancer, B8, which successfully restored hearing of *Slc26a5* knockout mice.

INTRODUCTION

Hearing loss is the most common form of sensory impairment, affecting over 400 million people worldwide of which 34 million are children.[1] Genetic mutations account for about 60% of all congenital hearing loss,[2–5] and over 100 non-syndromic hearing loss genes have been identified to date (https://hereditaryhearingloss.org/). Adeno-associated virus (AAV)-mediated gene therapy has emerged as a promising strategy for treating inherited and genetic disorders, including hereditary hearing loss.[4,6] Recent clinical trials have demonstrated the successful restoration of hearing function in children with recessive deafness DFNB9 through the use of a dual-vector strategy to deliver otoferlin (OTOF).[7–9] Meanwhile, studies have reported several successful hearing restorations of hereditary deafness

in animal models with gene therapy.[10] Despite the promise of AAVs due to their efficiency and low immunogenicity,[11] there are significant concerns regarding the safety of high-dose AAV administration. Issues such as hepatotoxicity from off-target transfection of the liver, thrombotic microangiopathy (TMA), and the risk of hepatocellular carcinoma associated with genomic integration of AAVs are notable challenges.[12–16] To mitigate these risks, improving the efficiency and specificity of AAVs while minimizing off-target effects and reducing required doses is crucial.

The *Myo15* promoter,[17] which targets hair cells (HCs) in the inner ear, is the best-characterized inner-ear-cell-specific promoter and has been widely used for gene therapy of hereditary hearing loss, both in pre-clinical and clinical research.[7,8,18,19] However, the intricate nature of the cochlea significantly

challenges the precise targeting of gene delivery. As a highly polarized and organized organ, the cochlea hosts multiple cell types, such as HCs, which are subdivided into outer HCs (OHCs) and inner HCs (IHCs), as well as supporting cells (SCs) and spiral ganglion neurons (SGNs).[20] Each cell type harbors unique cell-specific genes that are essential for hearing. For instance, IHCs specifically express hearing loss genes *Otof* and *Slc17a8* (*vGlut3*),[21,22] whereas OHCs express *Slc26a5*, which encodes the motor protein prestin.[23–26] Additionally, both IHCs and OHCs express a series of pan-HC markers, such as *Tmc1*,[27] *Myo7a*,[28] and *Atoh1*.[29,30] The sophisticated nature of the cochlea exemplifies the exquisite regulation involved in organ development; however, it significantly complicates the precise targeting of gene delivery.

Transcriptional enhancers orchestrate precise spatial and temporal control of gene expression during development and dictate cell fate determination.[31,32] The importance of these elements is further underscored by the fact that variants within these non-coding regulatory sequences are implicated in the etiology of various diseases.[33] However, the transcriptional regulation of cochlear genes remains largely unexplored. Although newly established methodologies, such as chromatin immunoprecipitation sequencing (ChIP-seq),[34] assay for transposase-accessible chromatin with high throughput sequencing (ATAC-seq),[35] and CRISPR-based high-throughput strategies,[36–38] have provided unprecedented tools for identifying transcriptional enhancers, a conclusive demonstration and mechanistic understanding of these elements generally rely on functional assessment through *in vivo* experiments. Additionally, the extremely low number of HCs and complex architecture of the cochlea have significantly limited the accessibility of these technologies. To date, only ChIP-seq and ATAC-seq studies on immature mouse HCs have been conducted.[39–41] Establishing a reliable approach to identify and dissect transcriptional enhancers of cochlear genes, particularly those associated with hearing loss genes, will significantly facilitate our understanding of gene regulation governing cochlea development and lay the foundation for developing effective and targeted gene therapies for hereditary hearing loss.

In this study, we introduce an AAV-reporter-based *in vivo* transcriptional enhancer reconstruction (ARBITER) workflow, which can be generally applied for the fast and reliable dissection of enhancers of hearing loss genes. With ARBITER, we successfully identified and characterized the enhancers for OHC-specific *Slc26a5*, which encodes the motor protein prestin,[23–26] and for the HC-specific *Myo7a*, which is associated with Usher syndrome.[28] We demonstrated that conserved non-coding elements (CNEs) within the gene loci functioned as transcriptional enhancers. In particular, two CNEs located in the intron of *Slc26a5*, designated as *Slc26a5*-E1 and E2, collaboratively control the precise and robust expression of *Slc26a5*. Functional investigations using knockout mouse models revealed that deletion of *Slc26a5*-E1 resulted in progressively reduced prestin expression and hearing loss. Simultaneous deletion of both *Slc26a5*-E1 and E2 completely eliminated the expression of prestin, leading to severe deafness. Additionally, we assessed the potential of using cell-specific enhancers in gene therapy for hereditary hearing loss with a *Slc26a5* dysfunction mouse model. Our results indicated that the originally identified

Slc26a5-E1 + E2 enhancer was suboptimal for restoring hearing sensitivity in the *Slc26a5* knockout mice due to its insufficient activity. To overcome this limitation, we dissected the key elements within *Slc26a5*-E1 and E2 using ARBITER and demonstrated that the most conserved modules were essential for gene expression. By reassembling these key modules, we engineered a highly efficient, OHC-specific synthetic enhancer, termed B8. B8-enhancer-mediated *Slc26a5* delivery drove prestin expression in a manner closely mimicking the native expression pattern and successfully restored hearing in *Slc26a5* knockout mice. Our findings provide a generalized approach for deciphering the enhancers of genes associated with hearing loss and offer a promising therapeutic strategy for the treatment of hereditary hearing loss with improved specificity, safety, and effectiveness.

RESULTS

Establishment of ARBITER

The concept behind the ARBITER workflow was to use the AAV-ie vector,[42] which efficiently infects multiple types of inner ear cells to deliver reporters containing synthetic gene regulatory elements to the cochlea. If the elements were indeed necessary for gene expression, the reporter carried by the AAV vector would exhibit a comparable expression pattern to that of the target gene (Figure 1). Initially, we delivered the AAV-ie reporter, which carries a ubiquitous cytomegalovirus enhancer fused chicken β-actin and β-globin (CAG) promoter, to the cochleae of neonatal mice via round window injection (RWI) at a dose of 1e10 genome copies (gc) per mouse. Tissues were collected 2 weeks later for immunofluorescence staining. The results showed that the AAV-ie vector, combined with the CAG promoter, efficiently transduced cochlear cells (Figure S1A), achieving nearly 100% transduction efficiency in HCs and 80%–95% in SCs (Figure S1B). Also, AAV-ie efficiently transduced vestibular HCs and SCs (Figures S1C and S1D). Additionally, administering AAV-ie with the CAG promoter at neonatal stage resulted in expansive infection of the brain (Figure S1E), as well as the heart and liver (Figure S1F). These results indicated that AAV-ie was well-suited for delivering reporters into the cochlea for dissecting the regulatory elements.

To select candidate regulatory elements, we identified open chromatin sequences and transcription factor (TF)-binding sequences near the gene loci of target genes by analyzing previously published ATAC-seq and ChIP-seq datasets from HCs (GEO: GSE181311 and GSE150000).[39,40] Sequences located within 2−200 kb upstream or downstream of the transcription start site (TSS) were considered potential regulatory elements (Figure 1A). We also chose CNEs in the gene loci that are deemed indispensable for normal development and strongly associated with *cis*-regulatory enhancers.[43–46] We used a genome browser (http://genome.ucsc.edu)[47,48] to analyze conservation across species, and conserved non-coding sequences exceeding 100 bp in length within the gene loci (from 50 kb upstream of TSS to 50 kb downstream of the last exon) were selected as candidate CNEs for further validation (Figure 1A). Subsequently, based on the selected elements, a series of reporter constructs were designed by individually or combinatorically cloning these elements into a reporter plasmid, with a synthetic minimal promoter (MinP) that retains basic promoter
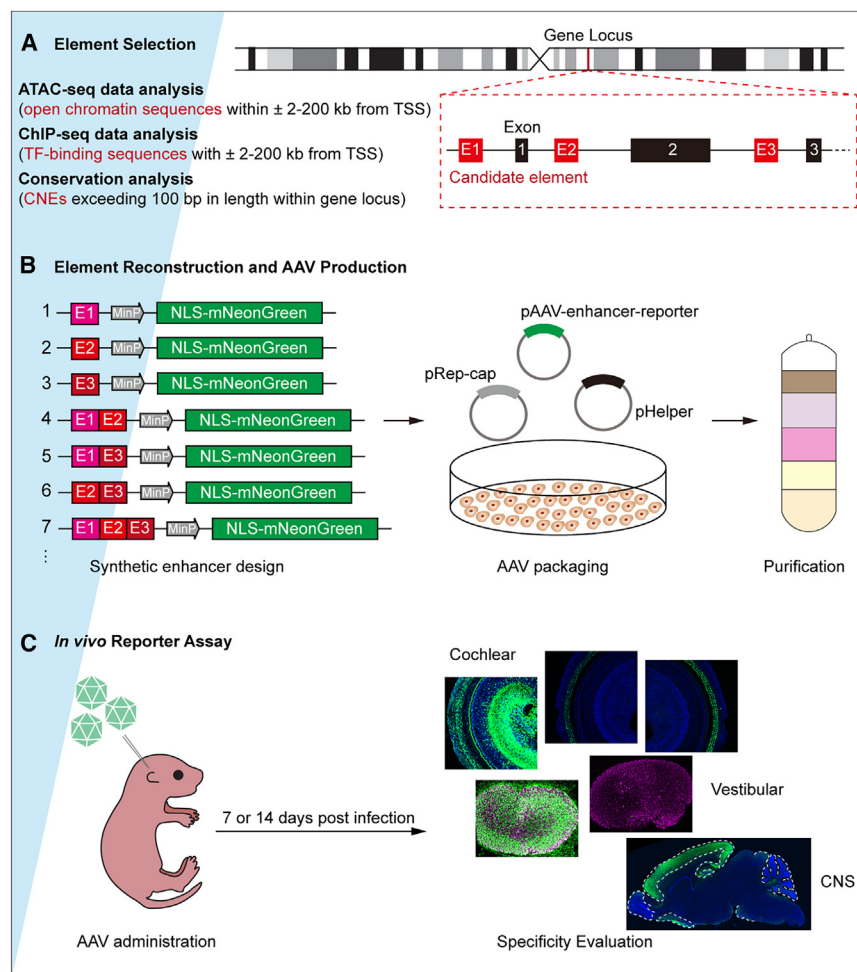
Figure 1. Concept and workflow of ARBITER

(A) Candidate regulatory elements were selected based on ATAC-seq data or ChIP-seq data or by analyzing the conserved non-coding elements (CNEs) across species. Open chromatin sequences or transcription factor (TF)-binding sequences within 2−200 kb upstream or downstream of gene transcription start site (TSS) and CNEs longer than 100 bp within the gene locus were selected as potential regulatory elements.

(B) Based on these elements, a series of reconstructed enhancers were designed by cloning the sequences into a pAAV-reporter plasmid individually or in a combined manner, then pAAV-enhancer-reporter plasmids were co-transfected with pRep-cap and pHelper plasmids into HEK293T cells to package AAVs, and then purified using iodixanol gradient.

(C) Purified AAVs were then individually delivered into the cochleae of neonatal mice through round window injection (RWI), and immunostaining and fluorescence imaging were performed to evaluate the specificity, efficiency, and intensity of the introduced elements in targeting cochlear and vestibular cells, as well as their effects on the central nervous system.

See also Figure S1.

activity,[49,50] fused downstream to initiate basal gene expression. AAV-ie vectors carrying the reporters were packaged and purified (Figure 1B). These purified AAV reporters were further individually administered to the cochleae of neonatal mice by RWI. After 1 or 2 weeks, the animals were euthanized and the specificity, efficiency, and intensity of the synthetic elements were evaluated using fluorescence imaging (Figure 1C).

To test the feasibility of the ARBITER approach, we first dissected the well-defined enhancers of *Atoh1*, which is necessary for HC development.[29,30] Three *Atoh1* enhancer elements that collaboratively regulate the expression of *Atoh1*, *Atoh1*-E1 to *Atoh1*-E3, have been identified using ATAC-seq (Figure S1G).[39] Based on these elements, we generated seven reporters, *At*-1 to *At*-7 (Table S2). Because *Atoh1* levels were high in cochlear HCs in the perinatal stage and started to decline significantly within the first week after birth,[51] we injected these vectors to the cochleae of post-natal day 1 (P1) mice at a dose of 2e10 gc per mouse and collected samples at P7. Subsequent evaluations showed that a single element only induced relatively low levels of gene expression in HCs, whereas combinations of these elements significantly improved the efficiencies (Figures S1H and S1J). Among them, *At*-6, the combination of *Atoh1*-E2 and E3, showed the best efficiency and specificity of targeting HCs,

whereas addition of E1 to *At*-6 (*At*-7) reduced the efficiency (Figures S1H and S1J). These results were consistent with the previous observation that *Atoh1*-E1 deletion did not affect HC development.[39] Additionally, these synthetic enhancers also induced specific gene expression in vestibular HCs (Figures S1I and S1J). Collectively, these results suggested that ARBITER was a reliable and efficient approach for dissecting the regulatory elements of cochlear genes.

CNEs within gene loci served as transcriptional enhancers of *Slc26a5* and *Myo7a*

We next attempted to identify transcriptional enhancers of hearing loss genes using ARBITER. We first focused on *Slc26a5*, which exhibits specific expression in OHCs and encodes the motor protein prestin.[23–26] Because previously published ATAC-seq data from the HCs of neonatal mice did not identify open chromatin regions within the gene locus of *Slc26a5*,[39–41] we analyzed CNEs in the *Slc26a5* locus because CNEs have been widely assumed to be essential for gene regulation due to their extreme conservation across different species.[43–46] We used a genome browser (http://genome.ucsc.edu)[47,48] to identify two CNEs of 247 and 525 bp in length, located within the intronic regions of *Slc26a5* (Figures 2A and S2A). Sequence alignment across nine species confirmed that *Slc26a5*-E1 and *Slc26a5*-E2 were highly conserved (Figure 2B). As negative controls, we also selected two non-conserved sequences, *Slc26a5*-E3 and *Slc26a5*-E4, which were 308 and 489 bp in length, respectively (Figure 2A). We
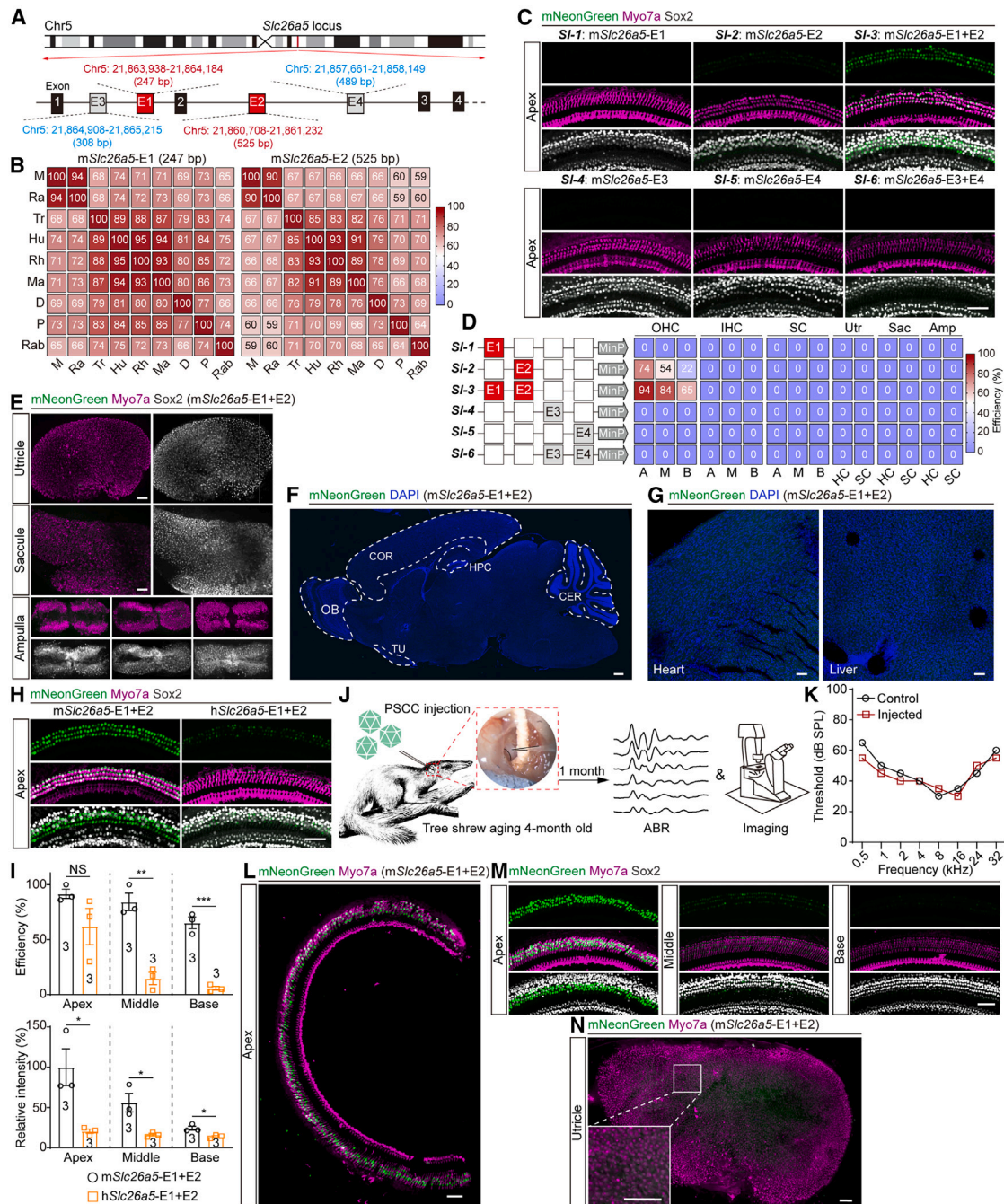
Figure 2. Dissecting enhancers of *Slc26a5*

(A) Schematic representation delineating candidate regulatory elements associated with the *Slc26a5* gene. Two CNEs, *Slc26a5*-E1 and E2, locating within introns 1 and 2, were selected as the candidate elements. Meanwhile, two non-conserved sequences, E3 and E4, were selected as negative controls.

(B) Sequence alignment identity of *Slc26a5*-E1 and E2 across species. M, mouse; Ra, rat; Tr, tree shrew; Hu, human; Rh, rhesus; Ma, marmoset; D, dog; P, pig; Rab, rabbit.

(C) Representative fluorescence images of infected cochlear cells in the apical region by the reconstructed enhancers derived from *Slc26a5*. AAV reporters were delivered to the cochlea of P2 mice at a dose of 1e10 gc per mouse, and samples were collected at P16 for analysis.

(D) Quantification of the transduction efficiencies of the *Slc26a5*-derived elements in cochlear and vestibular cells. Average transduction efficiencies from three independent experiments in each group were presented as a heatmap and labeled in the matrix.

(E) Transduction of vestibular cells by m*Slc26a5*-E1 + E2.

(F) Representative image of m*Slc26a5*-E1 + E2 infected brain. COR, cortex; HPC, hippocampus; OB, olfactory bulb; TU, tuber cinereum; CER, cerebellum.

(G) Representative image of m*Slc26a5*-E1 + E2 infected heart and liver.

(legend continued on next page)

designed the synthetic AAV reporters (*Sl*-1 to *Sl*-6) (Table S2) and administered them to the cochleae of P2 mice at a dose of 1e10 gc per mouse. *In vivo* evaluations of the transduced cochleae at P16 demonstrated that *Slc26a5*-E2 (*Sl*-2) alone was able to drive OHC-specific gene expression (Figures 2C and 2D). Moreover, when combined with *Slc26a5*-E1 (*Sl*-1), which did not induce gene expression, the transduction efficiency was significantly improved (Figures 2C and 2D). Consistent with the hypothesis that CNEs were essential for gene expression, neither single *Slc26a5*-E3 (*Sl*-4) and *Slc26a5*-E4 (*Sl*-5) nor their combination (*Sl*-6) resulted in OHC transduction (Figures 2C and 2D). Testing of *Slc26a5*-E1 + E2 (*Sl*-3) showed that *Sl*-3 induced little expression in other cochlear cell types (Figure 2D) or vestibular cells (Figures 2D and 2E). Besides, *Slc26a5*-E1 + E2 (*Sl*-3) did not induce off-target infection of the brain (Figure 2F), the heart, or the liver (Figure 2G).

We hypothesized that these CNEs work across species. We first engineered a human homologous enhancer, h*Slc26a5*-E1 + E2, and assessed its ability to induce OHC-specific transduction in a mouse model. Results showed that h*Slc26a5*-E1 + E2 was able to selectively transduce OHCs, albeit with lower efficiency and intensity compared with m*Slc26a5*-E1 + E2 (Figures 2H and 2I). We simultaneously adopted a genetically closed model of primates, the tree shrew,[52–55] whose cochlear structure and turns (3.0–3.5 cycles)[56] are closer to those of humans (2.5–3.0 cycles)[57] as compared with mice (1.5 cycles). We performed specificity evaluation of m*Slc26a5*-E1 + E2 by delivering AAV-ie reporter carrying m*Slc26a5*-E1 + E2 into the cochlea of a 4-month-old tree shrew through posterior semicircular canal (PSCC) injection, and auditory brainstem response (ABR) and fluorescence imaging tests were conducted 1 month later (Figure 2J). ABR tests revealed that AAV delivery did not lead to hearing impairments (Figure 2K). Fluorescence imaging demonstrated that m*Slc26a5*-E1 + E2 induced OHC-specific gene expression, especially in the apical region (Figures 2L and 2M), without off-target expression in vestibular cells (Figure 2N). These observations indicated that the CNEs identified, *Slc26a5*-E1 and E2, served as the transcriptional enhancers and collaboratively control the precise and robust expression of *Slc26a5*.

We then questioned whether ARBITER is a generalized approach for dissection of enhancers of hearing loss genes. To test this, we moved to another gene, *Myo7a*,[28] which is associated with Usher syndrome. Using similar strategies, we identified three CNEs locating within the gene locus of *Myo7a* (Figure S3A). Based on these elements, seven synthetic enhancers, *My*-1 to *My*-7 (Table S2), were designed and evaluated *in vivo*. AAV

reporters were administered at a dose of 1e10 gc per mouse to the cochleae of P2 mice and tissues were dissected after 2 weeks for evaluation. Results showed that *Myo7a*-E3 alone (*My*-3) induced cochlear and vestibular HC transduction specifically but with low efficiency (Figures S3B–S3D). However, when combined with *Myo7a*-E1 (*My*-1) or E2 (*My*-2), which did not induce gene expression, the efficiencies in cochlear and vestibular HCs were significantly increased (*My*-5 to *My*-7) (Figures S3B–S3D). These data suggested that the identified elements, *Myo7a*-E1 to E3, were responsible for the regulation of *Myo7a*. Collectively, our results demonstrated that ARBITER could be generally used for fast and reliable dissection of enhancers of hearing loss genes.

Slc26a5-E1 and E2 are essential for the expression of *Slc26a5*

To confirm the function of CNEs in regulating gene expression, we attempted to validate the function of our identified *Slc26a5* enhancers using knockout mouse models. Using CRISPR-Cas9-mediated gene editing, we successfully created *Slc26a5*-E1 knockout mice (*Slc26a5*-E1$^{-/-}$E2$^{+/+}$) and *Slc26a5*-E1 + E2 double knockout mice (*Slc26a5*-E1$^{-/-}$E2$^{-/-}$) and performed phenotype characterization (Figure 3A). We monitored the expression of prestin from P6, when prestin expression in OHCs is commenced,[58] using immunofluorescence staining. In a *Slc26a5*-E1 knockout mouse model, the expression of prestin in the apical, middle, or basal regions was not affected by either heterozygous or homozygous *Slc26a5*-E1 knockout at P6 and P16 (Figures S4A, S4B, and S4D). However, at P30, notable reductions in prestin levels were observed in the middle and basal regions of homozygous *Slc26a5*-E1 knockout mice (Figures S4C and S4D), and heterozygous knockout of *Slc26a5*-E1 led to moderate reductions in prestin levels compared with those of wild-type mice at P30 (Figures S4C and S4D). These observations suggested a progressive reduction in prestin expression during maturation following *Slc26a5*-E1 deletion, especially in the basal and middle turns of the cochlea. Scanning electron microscope (SEM) imaging at P30 revealed that *Slc26a5*-E1 deletion did not affect the morphology of OHCs (Figure S4E). Subsequent ABR and distortion product otoacoustic emission (DPOAE) tests across frequencies at P16, P30, and P90 demonstrated that the ABR and DPOAE thresholds of homozygous *Slc26a5*-E1 knockout mice were progressively increased from high frequencies to low frequencies as they matured (Figures S4F and S4G), indicating a progressive hearing loss. These findings revealed the crucial role of *Slc26a5*-E1 in prestin expression.

(H) Representative fluorescence images of infected cochlear cells in the apical region by m*Slc26a5*-E1 + E2 and h*Slc26a5*-E1 + E2.

(I) Statistics of transduction efficiencies and relative intensities of indicated element on targeting OHCs. Intensities were normalized to that of m*Slc26a5*-E1 + E2-driven gene expression in apical OHCs. *n* number in each group was labeled in or above the column.

(J) Schematic illustration of experiments in a tree shrew model. AAV-ie reporter carrying m*Slc26a5*-E1 + E2 was delivered into the cochlea of a 4-month-old tree shrew; auditory function tests and fluorescence imaging tests were performed 1 month later.

(K) Comparisons of ABR thresholds across frequencies between control and AAV-injected animals.

(L) Overall view of infected cochlear cells in the apical region by m*Slc26a5*-E1 + E2 in a tree shrew.

(M) Representative fluorescence images of infected cochlear cells in the apical, middle, and basal regions by m*Slc26a5*-E1 + E2.

(N) Representative fluorescence images of infected utricle cells by m*Slc26a5*-E1 + E2 in a tree shrew. Scale bar, 50 μm. Data were shown as mean ± SEM, *$p < 0.05$, **$p < 0.01$, ***$p < 0.001$. NS, no significance. Group differences were analyzed by unpaired two-tailed t test.
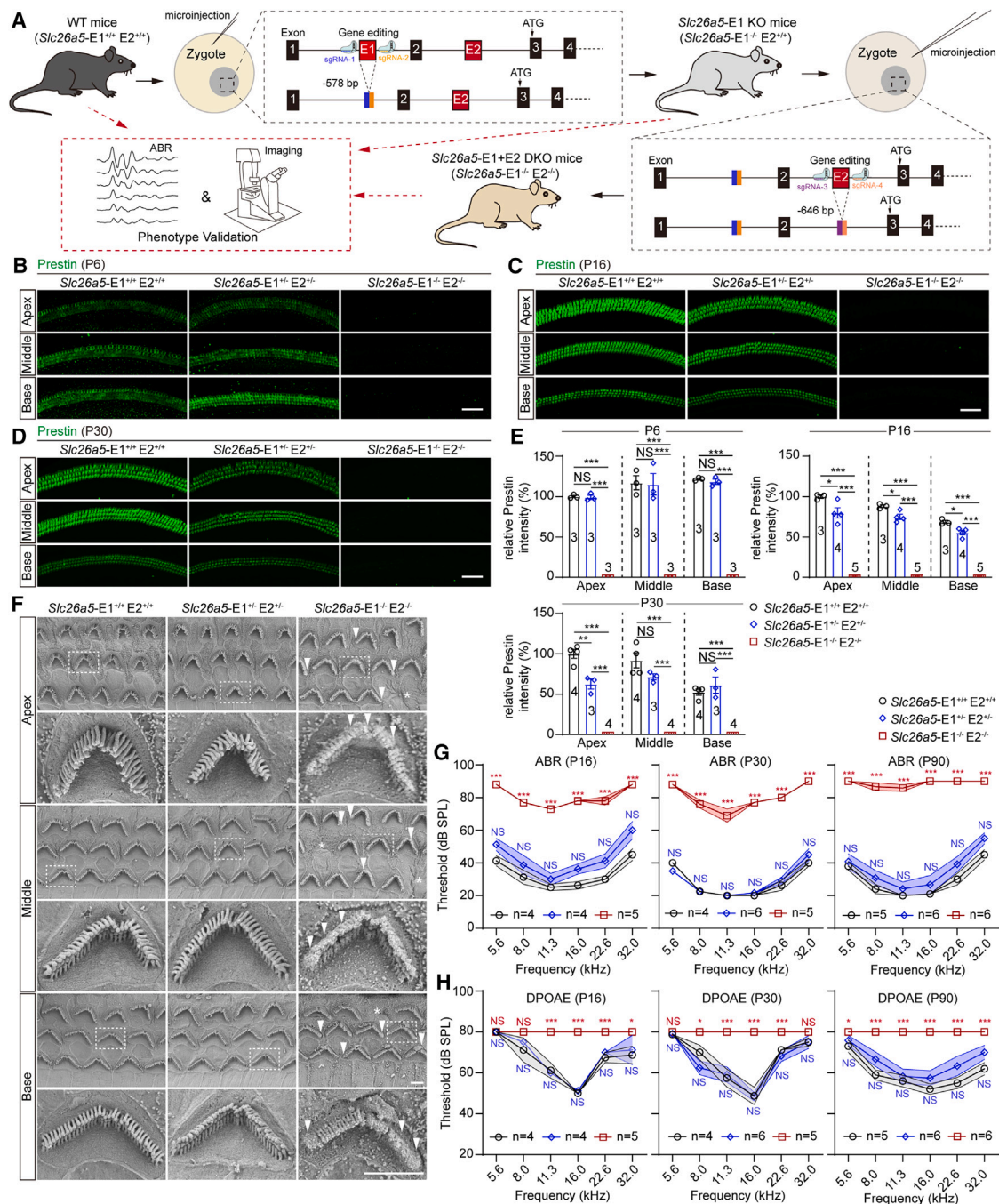
See also Figures S2 and S3.

Figure 3. Phenotype characterization of *Slc26a5*-E1 + E2 double knockout mice

(A) Illustration of the generation of *Slc26a5*-E1 knockout and *Slc26a5*-E1 + E2 double knockout mice and related phenotype validation. Single-guide RNAs (sgRNAs) targeting the upstream and downstream regions of *Slc26a5*-E1 were designed and co-injected with the CRISPR-Cas9 protein into one-cell-stage zygotes. After editing at the target sites, non-homologous end joining repair (NHEJ) resulted in the loss of *Slc26a5*-E1. Using *Slc26a5*-E1 knockout mice as the background, sgRNAs targeting the upstream and downstream of *Slc26a5*-E2 were similarly designed and injected into one-cell-stage zygotes, together with the CRISPR-Cas9 protein for gene editing. Auditory function and prestin expression levels in OHCs were evaluated for all the mouse strains.

(B–D) Representative cochlear immunostaining of prestin in the apical, middle, and basal regions of wild-type, heterozygous *Slc26a5*-E1 + E2 knockout, and homozygous *Slc26a5*-E1 + E2 knockout mice at P6 (B), P16 (C), and P30 (D). Scale bar, 50 μm.

(E) Relative prestin intensities in the apical, middle, and basal regions of indicated mice at P6, P16, and P30. Intensities were normalized to the apical prestin intensities of wild-type mice at indicated time. *n* number in each group was labeled in the column.

(F) Representative SEM images of OHCs in the apical, middle, and basal regions from indicated mice at P30. The white asterisks indicated the missing OHCs, the white arrows indicated the fused stereocilia bundles. Scale bar, 2.5 μm.

(legend continued on next page)

We next assessed the expression of prestin in *Slc26a5*-E1 + E2 double knockout mice. Strikingly, homozygous knockout of *Slc26a5*-E1 + E2 completely abolished the expression of prestin (Figures 3B–3E), highlighting the crucial role of *Slc26a5*-E1 and E2 in prestin regulation. SEM imaging at P30 revealed that homozygous knockout of *Slc26a5*-E1 + E2 resulted in significant OHC damage, with obvious OHC loss and stereocilia fusion in the apical, middle, and basal regions (Figure 3F). In line with these observations, ABR and DPOAE tests showed that homozygous knockout of *Slc26a5*-E1 + E2 led to significant ABR threshold elevation (Figure 3G) as well as DPOAE abolishment (Figures 3G and 3H). Together with previous findings showing that deletion of intron 2, which covered the sequence of *Slc26a5*-E2, led to delayed gene expression during OHC maturation,[59] these results revealed that the collaboration of two enhancer elements was essential to ensure the robust expression of target genes.

Expression from the *Slc26a5*-E1 + E2 enhancer is specific but insufficient for gene therapy

We questioned whether our identified enhancers could be used for gene therapy of hereditary hearing loss. The most common non-syndromic hereditary hearing loss is caused by dysfunctional mutations or is autosomal recessive[6,60]; to model this, we employed a *Slc26a5* knockout mouse model whose *Slc26a5* expression was inactivated through CRISPR-mediated base editing.[61] We attempted to deliver *Slc26a5* using the broad CAG promoter.[42] AAV-ie-CAG-*Slc26a5* at a dose of 1e10 gc per mouse was administered at P3 through RWI, and functional tests and imaging experiments were performed at P30. AAV-ie-CAG-*Slc26a5* delivery restored the expression of prestin in the OHCs (Figures S5A and S5B). However, the prestin intensities of rescued mice were much lower than those in wild-type mice (Figure S5C). Moreover, gene delivery using the CAG promoter induced ectopic prestin expression in IHCs and vestibular HCs, suggesting potential side effects and safety risks (Figures S5A and S5D). Subsequent ABR and DPOAE tests showed that gene therapy using AAV-ie-CAG-*Slc26a5* did not significantly restore the hearing sensitivity of *Slc25a5*^−/− mice (Figure S5E). Individually analyzing the hearing function of the rescued mice showed that only two out of 11 treated mice showed partial improvement in ABR response and one out of 11 treated mice showed a recovery in DPOAE response (Figure S5F). These observations were consistent with our previous results indicating that gene therapy using the CAG promoter failed to restore the hearing sensitivity of *Slc25a5*^−/− mice efficiently.[62]

We next performed gene therapy using the identified OHC-specific enhancer, *Slc26a5*-E1 + E2. Safety of the enhancer for gene delivery was first assessed. SEM imaging (Figure S5G) and auditory function tests (Figures S5H–S5K) indicated that the *Slc26a5*-E1 + E2 enhancer was safe for gene delivery. We

next delivered the *Slc26a5* gene into the cochleae of *Slc25a5*^−/− mice using the *Slc26a5*-E1 + E2 enhancer. AAV-ie-E1 + E2-*Slc25a5*, at a dose of 1e10 gc per mouse, induced OHC-specific (albeit low) prestin expression (Figures 4A–4C). We increased the dose to 5e10 gc per mouse and saw a more robust prestin expression (Figures 4A–4C). Moreover, neither low-dose nor high-dose AAV-ie-E1 + E2-*Slc25a5* caused ectopic expression of prestin in IHCs (Figure 4A) or vestibular HCs (Figure 4D), highlighting the advantages of cell-specific enhancers in targeted gene therapy. However, the prestin levels in these treated mice remained significantly lower than those in wild-type mice (Figure 4C). We assessed the hearing function of the treated mice. ABR waveforms at 16 kHz showed that rescue mediated by high-dose AAV-ie-E1 + E2-*Slc26a5* partially restored hearing function, whereas low-dose AAV-ie-E1 + E2-*Slc26a5* did not yield significant improvements (Figure 4E). Waveform analysis at 90 dB sound press level (SPL) demonstrated that none of the treatments restored wave 1 amplitudes and latencies (Figure 4F). Further ABR and DPOAE analysis showed that neither dose significantly restored hearing function (Figure 4G). Analysis of hearing function in individual treated mice showed that only 3 out of 12 high-dose-treated mice showed partial improvement in ABR responses, and two out of 12 high-dose-treated mice showed some recovery in DPOAE responses (Figure 4H). These findings highlighted the advantages of *Slc26a5*-E1 + E2 for targeted gene delivery but showed that low activity still limited the use of *Slc26a5*-E1 + E2 as a therapeutic tool.

Conserved elements within *Slc26a5*-E1 + E2 enhancer segments can drive gene expression

To overcome the low level of expression from the *Slc26a5*-E1 + E2 enhancer, we attempted to modify the original enhancers using ARBITER to achieve a higher expression level while preserving OHC specificity. We first asked whether there exist essential sequences within the enhancer. To address this, we divided the E1 and E2 enhancers into small modules based on their length and conservation. E1 was split into three parts, namely E1P1 to E1P3, with E1P3 (93 bp) as the most conserved element (Figure S6A). E2 was split into four parts and designated as E2P1–E2P4, with E2P2 (132 bp) and E2P3 (128 bp), respectively, being the most conserved elements (Figure S6B). We first evaluated the efficiencies of each individual module on transducing OHCs and found that none of them resulted in OHC-specific reporter expression (Figures S6C and S6D). Because our initial reconstruction results showed that combining *Slc26a5*-E1 and E2 synergized the transduction efficiency, we designed a series of synthetic enhancers by combining full-length E1 or E2 with modules derived from the other element (A series, A1 to A7) (Table S2) to test which modules were necessary for gene expression. AAV reporters carrying different synthetic enhancers were delivered at a dose of 1e10 gc per mouse, with the full-length E1 + E2 as a control. Subsequent evaluations showed

---

(G and H) ABR (G) and DPOAE (H) thresholds across frequencies of indicated mice at indicated time. *n* number in each group was labeled in the legend. ABR, auditory brainstem response; DPOAE, distortion product otoacoustic emission. Data were shown as mean ± SEM, *$p < 0.05$, **$p < 0.01$, ***$p < 0.001$; NS, no significance. Group differences were analyzed by unpaired two-tailed t test. For (G) and (H), differences between wild-type and heterozygous *Slc26a5*-E1 + E2 knockout mice were labeled in blue, differences between wild-type and homozygous *Slc26a5*-E1 + E2 knockout mice were labeled in red.
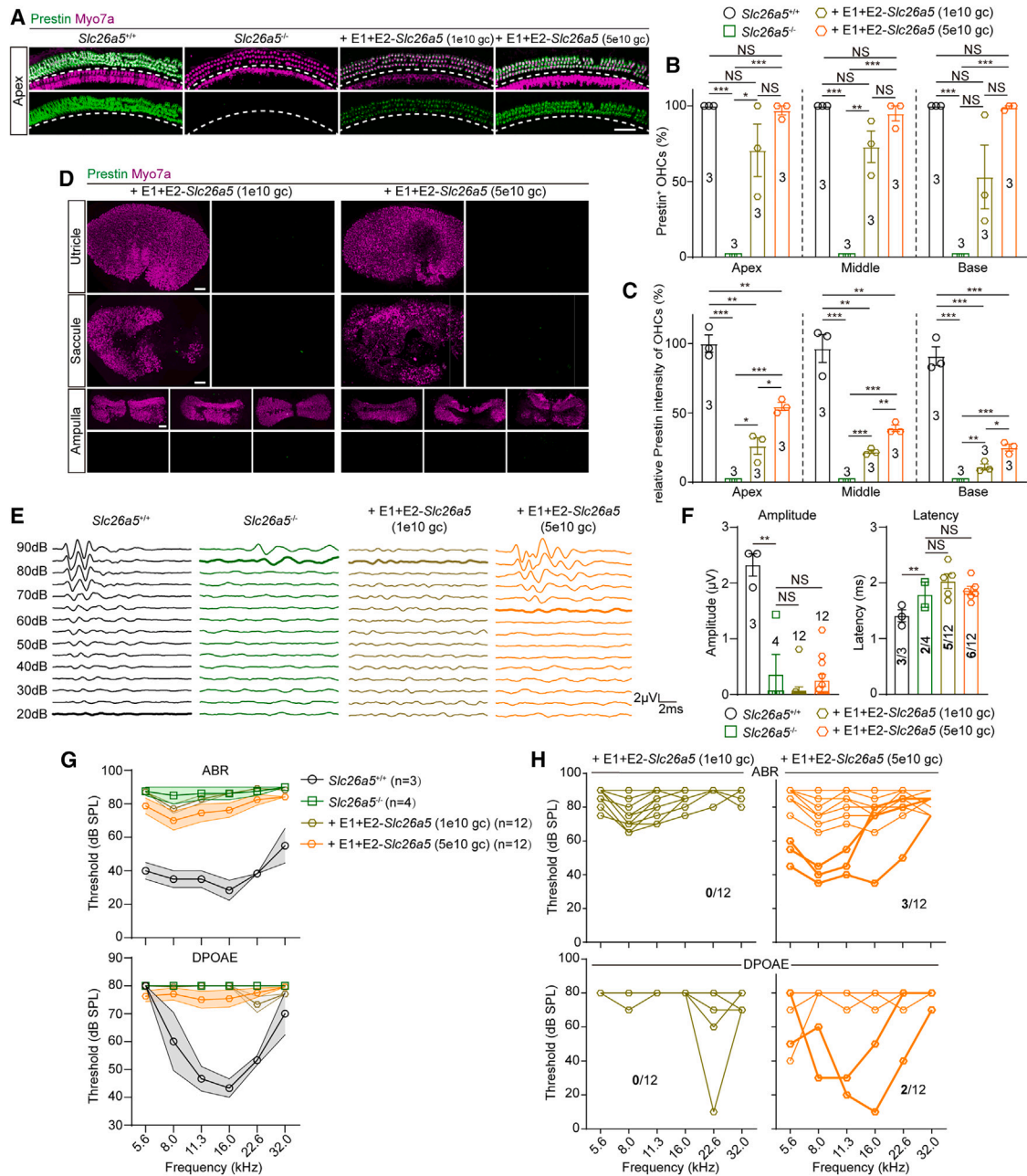See also Figure S4.

Figure 4. ***Slc26a5*-E1 + E2-enhancer-mediated gene therapy in *Slc26a5*$^{-/-}$ mice**

(A) Representative cochlear immunostaining of prestin and Myo7a in the apical regions of mice from indicated group. AAV vectors were administered to the cochleae of *Slc26a5*$^{-/-}$ mice at P3, and samples were collected at P30.

(B and C) Statistics of prestin$^+$ OHC populations (B) and relative prestin intensities of OHCs (C) in the apical, middle, and basal regions. Prestin intensities were normalized to apical OHCs of WT mice. *n* number in each group was labeled in the column.

(D) Representative prestin staining in vestibular HCs after gene therapy using *Slc26a5*-E1 + E2 enhancer at indicated doses.

(E) Representative ABR waveforms at 16 kHz across all sound pressure levels; the bold line indicated the ABR thresholds.

(F) Statistics of peak amplitudes and latencies of ABR wave 1 evoked at 16 kHz by 90 dB SPL of mice from indicated group. *n* numbers in each group were labeled in the column, 2 out of 4 *Slc26a5*$^{-/-}$ mice, 5 out of 12 E1 + E2-*Slc26a5* (1e10 gc) rescued mice, and 6 out of 12 E1 + E2-*Slc26a5* (5e10 gc) rescued mice could be determined for their latencies.

(G) Comparisons of ABR and DPOAE thresholds across frequencies between mice from indicated group, *n* numbers in each group were labeled in the legend.

that, among the three synthetic sequences that were generated by combining E1 modules and full-length E2, A3 (E1P3 + E2) induced robust OHC transduction (Figures 5A and 5B). Meanwhile, A5 (E2P2 + E1) and A6 (E2P3 + E1), which were derived from the combination of most conserved modules in E2 with full-length E1, induced significant OHC transduction (Figures 5A and 5B). Further analyses revealed that transduction efficiencies correlated well in a linear manner with sequence conservation of split elements, both for modules derived from *Slc26a5*-E1 (Figure 5C) and from E2 (Figure 5D). Similarly, a good correlation was observed between reporter expression intensities and fragment conservation (Figures 5E and 5F). These findings indicated that the most highly conserved modules for *Slc26a5* were correlated with high expression.

Engineering of an efficient OHC-specific enhancer by reassembling key multipartite modules

We hypothesized that the key modules were sufficient for transcriptional regulation of *Slc26a5*. To test this idea, we designed a series of reporters by combining less-conserved fragments or more-conserved elements together to generate the B series (Table S2). *In vivo* evaluations showed that synthetic enhancers derived from more-conserved modules or the key modules, B5 (E1P3 + E2P2) and B6 (E1P3 + E2P3), transduced OHCs specifically (Figures S7A and S7B). Conversely, combinations of less-conserved elements, such as B1 (E1P1 + E2P1), B2 (E1P1 + E2P4), B3 (E1P2 + E2P1), and B4 (E1P2 + E2P4), did not induce OHC-specific reporter expression (Figures S7A and S7B). More importantly, B7 (E1P3 + E2P2 + E2P3), which was generated by combining one key module from E1 and two key modules from E2, sequentially, induced more efficient transduction than B5 and B6, which were derived from E1P3 and a single key element from E2 (Figures S7A and S7B). These results supported the notion that the smaller, key conserved modules are essential and sufficient to synergistically drive gene expression in mouse OHCs.

In accordance with this pattern, we further designed two synthetic enhancers by duplicating and combining the key modules and generated B8 and B9 (Table S2). B8 (E1P3 × 2 + E2P2 × 2 + E2P3 × 2) was created by sequentially combining double E1P3 with double E2P2 and double E2P3, and B9 ((E1P3 + E2P2 + E2P3) × 2) was generated by duplicating B7, regardless of the orientation of the original *Slc26a5*-E1 + E2 (Figure 6A). *In vivo* evaluations demonstrated that B8, which emulated the orientation of the original E1 + E2 enhancer, exhibited significantly improved gene expression in OHCs compared with E1 + E2 or B7 (Figures 6B and 6C). Notably, B8 demonstrated significantly improved efficiency, achieving almost 100% transduction of OHCs in the apical, middle, and basal regions (Figure 6C). Moreover, the levels of B8-mediated gene expression were also significantly enhanced (Figure 6C). Further imaging analyses of cochlear cross-sections (Figure 6D) and vestibular tissues (Fig-

ure 6E) confirmed that B8 was a highly specific enhancer targeting OHCs. Besides, B8 did not induce off-target infection of the brain (Figure 6F), the heart, or the liver (Figure 6G). We evaluated the safety of B8 for gene delivery. Similar to the original *Slc26a5*-E1 + E2 enhancer, AAV-ie-B8-nls-mNeonGreen did not alter the morphology of stereocilia in HCs (Figure 6H). Auditory function testing demonstrated that the B8 enhancer was safe for OHC-specific gene delivery (Figures 6I–6L). Thus, we successfully engineered a highly efficient, safe, and specific enhancer for OHC-targeting gene delivery.

Enhancer B8 successfully restores the hearing sensitivity of *Slc26a5* knockout mice

We then administrated two doses of AAV-ie-B8-*Slc26a5* (1e10 gc and 5e10 gc per mouse) to the cochleae of *Slc26a5*$^{-/-}$ mice via RWI at P3. Imaging experiments at P30 showed efficient expression of prestin in OHCs of mice treated with both doses (Figures 7A and 7B). Notably, the prestin intensities of treated *Slc26a5*$^{-/-}$ mice using the high-dose B8-*Slc26a5* reached comparable levels to those observed in wild-type mice, particularly in the apical region (Figure 7C). Moreover, the delivery of *Slc26a5* using the B8 enhancer did not result in mislocalization of prestin in IHCs (Figure 7A) or vestibular cells (Figure 7D). ABR waveforms at 16 kHz demonstrated that high-dose B8-*Slc26a5* treatment efficiently restored the ABR threshold of *Slc26a5*$^{-/-}$ mice to levels comparable with those of wild-type mice, whereas low-dose treatment partially improved hearing function (Figure 7E). Importantly, the wave 1 amplitudes and latencies evoked at 16 kHz by 90 dB of *Slc26a5*$^{-/-}$ mice were completely restored to similar levels as those of wild-type mice following high-dose B8-*Slc26a5* treatment (Figure 7F). Besides, ABR waveforms at other frequencies of high-dose B8-*Slc26a5*-treated mice were also intact (data not shown). When considering ABR and DPOAE responses of all treated mice in each group, we found that administration of AAV-ie-B8-*Slc26a5* at a dose of 5e10 gc per mouse efficiently restored the hearing function of *Slc25a5*$^{-/-}$ mice to levels comparable with those of wild-type mice (Figure 7G). Individual ABR analysis revealed significant improvement in ABR response for four out of eight mice treated with the low dose and eight out of 11 mice treated with the high-dose B8-*Slc26a5* (Figure 7H). DPOAE analysis showed that two out of eight mice treated with the low dose and six out of 11 mice treated with the high dose exhibited a recovery in DPOAE response (Figure 7H). Consistent with hearing function results, SEM imaging showed that rescue using the high-dose B8-*Slc26a5* fully restored the morphology of OHC stereocilia (Figure 7I). In contrast to our previous attempts to rescue the hearing function of *Slc25a5*$^{-/-}$ mice using the CAG promoter or the *Slc26a5*-E1 + E2 enhancer, which proved to be less effective, the synthetic B8 enhancer demonstrated superior efficacy for gene therapy. These findings underscored the significant advantages of employing highly efficient and specific enhancers

---

(H) Individual ABR and DPOAE thresholds across frequencies of gene-therapy-rescued mice using *Slc26a5*-E1 + E2 enhancer at indicated doses. The bold line indicated the thresholds of mice with significant functional restoration after gene therapy. The denominator indicated the number in each group and the numerator indicated the number of mice with significant functional restoration. Data were shown as mean ± SEM, *p < 0.05, **p < 0.01, ***p < 0.001; NS, no significance. Group differences were analyzed by unpaired two-tailed t test. Scale bar, 50 μm.
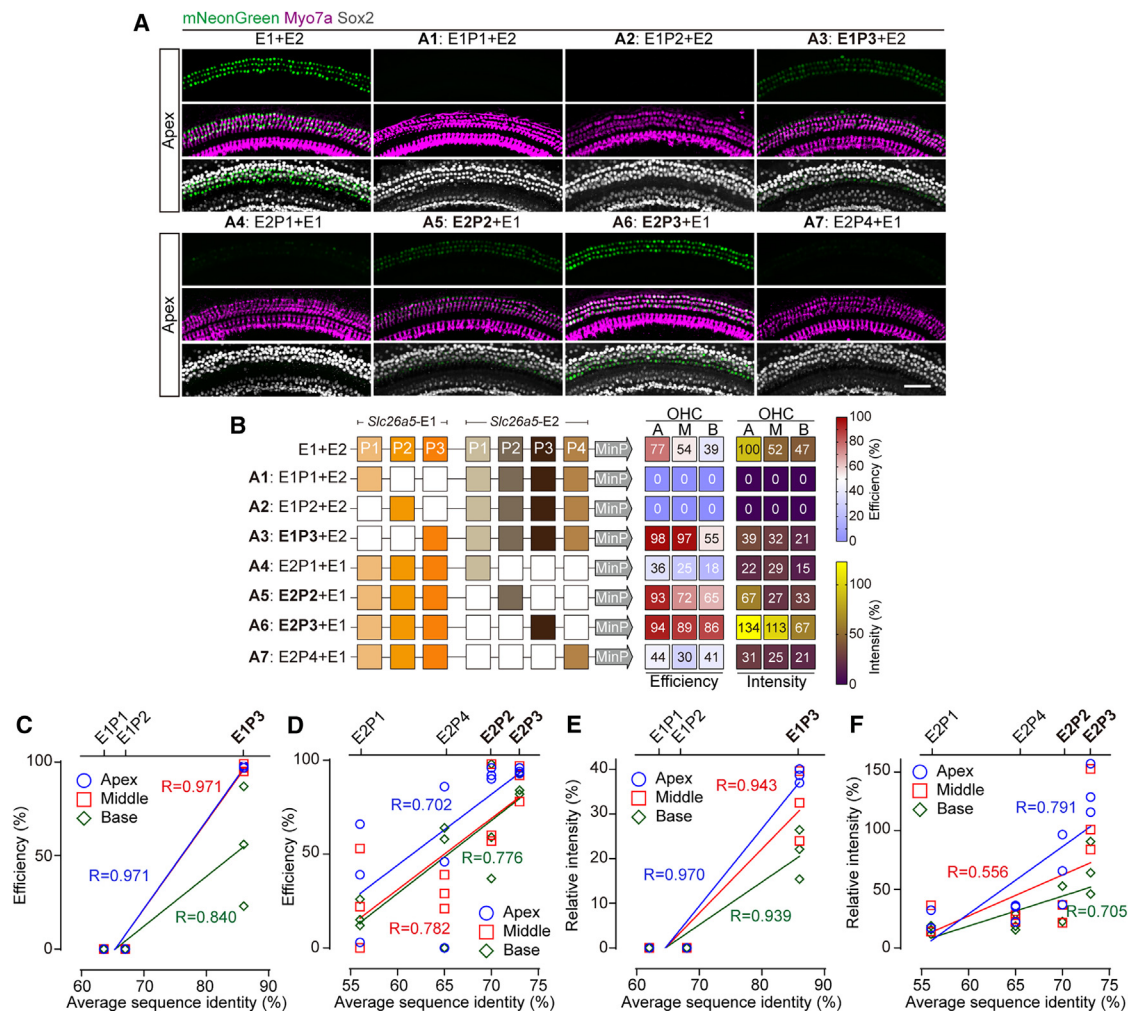See also Figure S5.

Figure 5. Dissecting the key elements within *Slc26a5*-E1 + E2 enhancer

(A) Representative fluorescence images of infected OHCs in the apical region by the indicated synthetic enhancers. AAV reporters were delivered to the cochlea of P2 mice at a dose of 1e10 gc per mouse, and samples were collected at P16 for analysis. Scale bar, 50 μm.

(B) Transduction efficiencies and relative gene expression intensities of indicated elements on targeting OHCs. Intensities were normalized to that of *Slc26a5*-E1 + E2-driven gene expression in apical OHCs. Average transduction efficiencies or relative intensities from three independent experiments in each group were presented.

(C and D) Correlation between transduction efficiencies and conservations of multipartite enhancers derived from E1 (C) and E2 (D); conservations were defined as the average sequence identities of indicated elements from different species (mouse, rat, tree shrew, human, rhesus, marmoset, dog, pig, and rabbit).

(E and F) Correlation between relative intensities and conservations of multipartite enhancers derived from E1 (E) and E2 (F).

See also Figure S6.

inspired by key regulatory modules for targeted gene therapy approaches.

OHC-specific gene delivery using B8 in adult mouse model

Newborn human inner ears are fully developed, whereas the mouse cochlea undergoes structural and functional changes from the neonatal to adult stages.[6,63] To evaluate the feasibility of B8 enhancer for potential clinical applications, we investigated the ability of B8 to transduce OHCs in adult mice. We adopted an AAV2 vector, which showed high efficiency in transducing mature HCs.[64] AAV reporters were administered into the

cochleae at P30, and functional and imaging testing were performed after 10 days (Figure 8A). Fluorescence imaging demonstrated that, compared with the CAG promoter that transduced both OHCs and IHCs, B8 induced specific gene expression in OHCs (Figures 8B and 8C). Moreover, B8 did not lead to off-target transduction in vestibular cells (Figure 8D). ABR testing showed comparable ABR thresholds at 16 kHz between control mice and AAV2-B8-nls-mNeonGreen-injected mice (Figure 8E), but an elevated threshold for AAV2-CAG-nls-mNeonGreen-injected mice (Figure 8E), which might be due to toxicity caused by the CAG-mediated strong expression of nls-mNeonGreen in IHCs. Additionally, CAG rather than B8-mediated delivery led
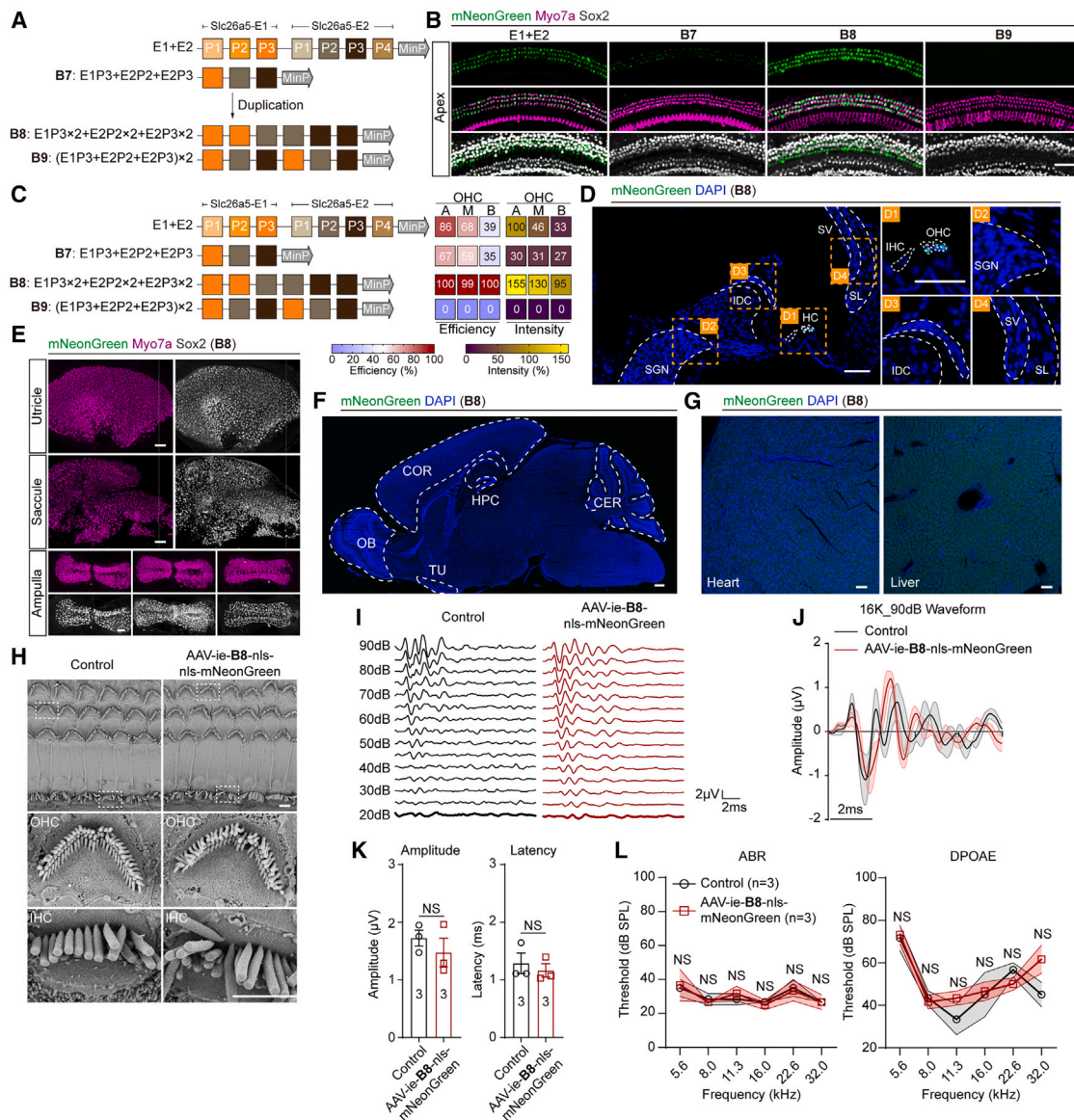
Figure 6. Engineering of efficient and OHC-specific enhancers

(A) Schematic illustration of strategies to reconstruct the multipartite enhancers.

(B) Representative fluorescence images of infected OHCs in the apical region by the indicated enhancers; the full-length *Slc26a5*-E1 + E2 enhancer was used as control. AAV reporters were administered at a dose of 1e10 gc per mouse, and samples were collected at P16 for analysis. Scale bar, 50 μm.

(C) Transduction efficiencies and relative gene expression intensities of indicated elements on targeting OHCs. Intensities were normalized to that of *Slc26a5*-E1 + E2-driven gene expression in apical OHCs. Average transduction efficiencies or relative intensities from three independent experiments in each group were presented.

(D) Representative cross-section image of AAV-ie-B8-nls-mNeonGreen-infected cochleae. HCs, hair cells; OHCs, outer HCs; IHCs, inner HCs; IDCs, interdental cells; SGNs, spiral ganglion neurons; SV, stria vascularis; SL, spiral ligament. Scale bar, 50 μm.

(E) Transduction of vestibular cells by AAV-ie-B8-nls-mNeonGreen. Scale bar, 50 μm.

(F) Representative image of AAV-ie-B8-nls-mNeonGreen-infected brain. COR, cortex; HPC, hippocampus; OB, olfactory bulb; TU, tuber cinereum; CER, cerebellum. Scale bar, 50 μm.

(G) Representative image of AAV-ie-B8-nls-mNeonGreen-infected heart and liver. Scale bar, 50 μm.

(H) Representative SEM images of HCs of cochleae whole mount prepared from control and AAV-ie-B8-nls-mNeonGreen-delivered mice. Scale bar, 2.5 μm.

(I) Representative ABR waveforms at 16 kHz across all sound pressure levels, the bold line indicated the ABR thresholds.

(J) Plot of ABR waveforms evoked at 16 kHz by 90 dB SPL from control and AAV-ie-B8-nls-mNeonGreen-delivered mice.

(K) Statistics of peak amplitudes and latencies of ABR wave 1 evoked at 16 kHz by 90 dB SPL from control and AAV-ie-B8-nls-mNeonGreen-delivered mice. *n* = 3 in each group.

(L) Comparisons of ABR and DPOAE thresholds across frequencies between control and AAV-ie-B8-nls-mNeonGreen-delivered mice. *n* = 3 in each group. Data were shown as mean ± SEM; NS, no significance. Group differences were analyzed by unpaired two-tailed t test.
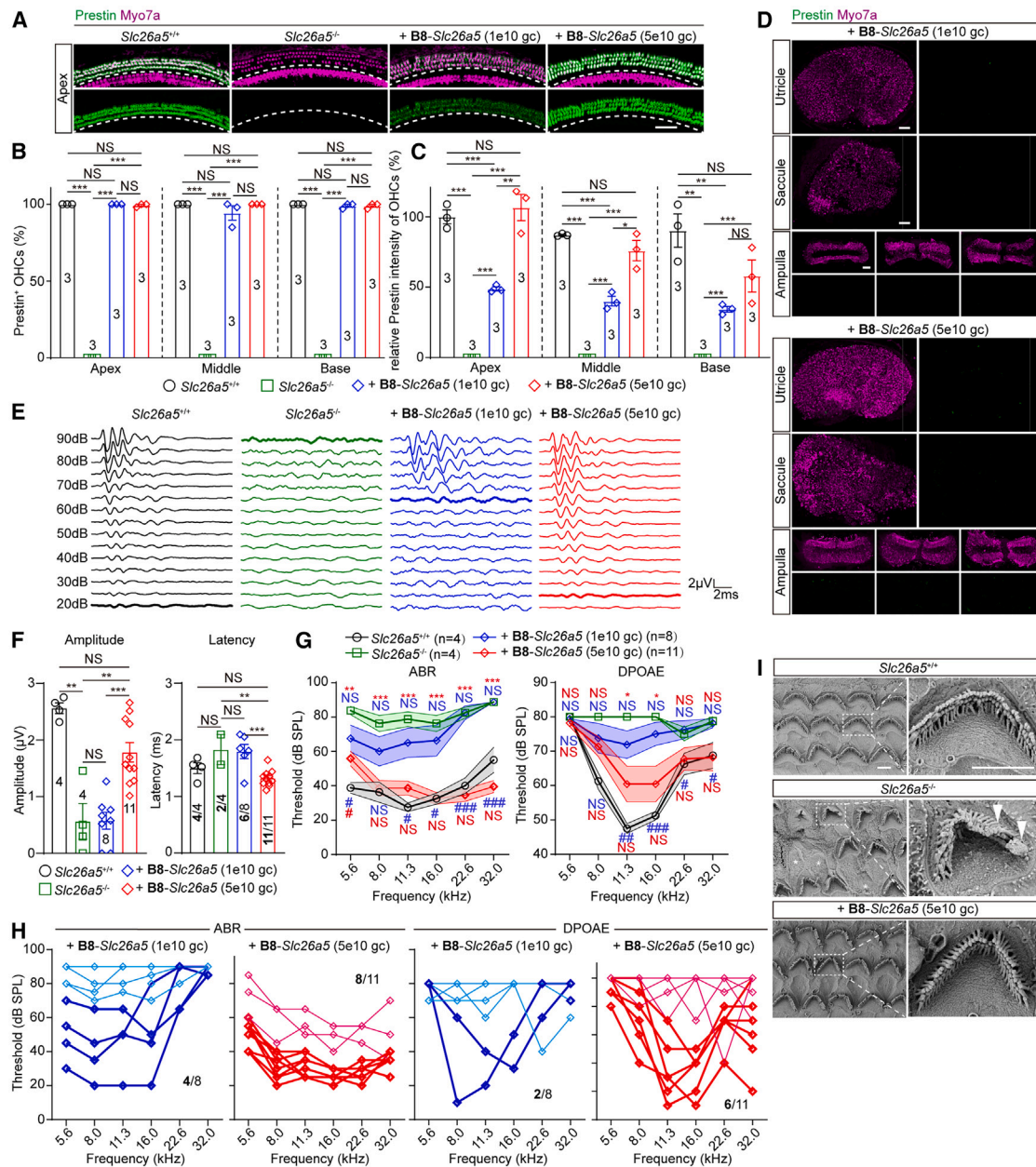
See also Figure S7.

Figure 7. B8 enhancer-mediated gene therapy in *Slc26a5*⁻/⁻ mice

(A) Representative cochlear immunostaining of prestin and Myo7a in the apical regions of mice from indicated group. AAV-ie-B8-*Slc26a5* was administered to the cochleae of *Slc26a5*⁻/⁻ mice at P3, and samples were collected at P30. Scale bar, 50 μm.

(B and C) Statistics of prestin⁺ OHC populations (B) and relative prestin intensities of OHCs (C) in the apical, middle, and basal regions. Prestin intensities were normalized to apical OHCs of WT mice. *n* number in each group was labeled in the column.

(D) Representative prestin staining in vestibular HCs after gene therapy using B8 enhancer at different doses. Scale bar, 50 μm.

(E) Representative ABR waveforms at 16 kHz across all sound pressure levels; the bold line indicated the ABR thresholds.

(F) Statistics of peak amplitudes and latencies of ABR wave 1 evoked at 16 kHz by 90 dB SPL of mice from indicated group. *n* numbers in each group were labeled in or above the column; 2 out of 4 *Slc26a5*⁻/⁻ mice, and 6 out of 8 B8-*Slc26a5* (1e10 gc) rescued mice could be determined for their latencies.

(G) Comparisons of ABR and DPOAE thresholds across frequencies between mice from indicated group; *n* numbers in each group were labeled in the legend. Differences between rescued mice (blue for B8-*Slc26a5* [1e10 gc] group and red for B8-*Slc26a5* [2e10 gc] group) and *Slc26a5*⁻/⁻ mice were labeled above the thresholds as asterisks. Differences between rescued mice and *Slc26a5*⁺/⁺ mice were labeled below the thresholds as hash.

(legend continued on next page)

to reduced wave 1 amplitudes and elongated latencies (Figure 8F). Finally, ABR across different frequencies showed similar thresholds between control mice and mice injected with AAV2-B8-nls-mNeonGreen (Figure 8G). These results indicated that B8 was safe and efficient for OHC-specific gene delivery in adult mice.

DISCUSSION

Congenital hearing loss occurs in approximately 1–3 out of 1,000 newborn babies worldwide, with up to 60% of all cases being associated with hereditary factors.[2–5] Currently, clinical treatments for hereditary hearing loss primarily involve the use of cochlear implants, which restore auditory function by directly stimulating neurons.[65] Unfortunately, this approach still has limitations in the perception of natural sound and hearing sensitivity, especially in noisy environment.[65] AAV-mediated gene therapy has emerged as a promising strategy for treating hereditary hearing loss, showing great potential in clinical trials.[7–9] However, significant concerns remain regarding the safety and specificity of AAV vectors. To date, more than 100 non-syndromic hearing loss genes have been identified, many of which are specifically expressed in certain cell types within the cochlea. The intricate nature of the cochlea further complicates the challenge of precisely targeting gene delivery. Although several AAV vectors that efficiently transduce cochlear cells, such as Anc80L65,[66] AAV2.7m8,[67] AAV9-PHP.B,[68] and AAV-ie[42] and its mutant AAV-ie-K558R,[62] have been developed in recent years, the underwhelming specificity of these vectors suggests potential side effects and safety risks.

Gene delivery using tissue- or cell-specific promoters/enhancers would minimize off-target expression of transgenes.[69] This strategy has found widespread application in clinical settings to treat genetic disorders across different tissues, such as the eye,[70] muscle,[71] and liver.[69] Given the sophisticated nature of the cochlea and the complexity of hearing loss genes, developing cochlear-cell-specific gene delivery approaches is urgently needed. Herein, we introduce the ARBITER workflow to decipher enhancers of hearing loss genes. Although the packaging size of AAV vectors limits the reconstruction of enhancers in a way that mimics their natural chromosomal environments—for instance, overlooking the spatial distance between individual elements, which could be important for gene regulation[72,73]—ARBITER represents a fast and reliable method for dissecting the transcriptional enhancers in an in vivo situation. With ARBITER, we successfully identified enhancers of Slc26a5. Two CNEs in the Slc26a5 gene locus, Slc26a5-E1 and E2, which are critical for regulating gene expression, were identified. We also dissected the enhancers of Myo7a, indicating that ARBITER can be used generally for other genes associated with hearing loss.

The establishment of ARBITER significantly advances our ability to identify cell-specific enhancers in the cochlea, thereby accelerating the development of targeted gene therapy for hereditary hearing loss.

ARBITER has also shown significant suitability for optimizing and engineering enhancers. In the case of Slc26a5, we illustrated that although the Slc26a5-E1 + E2 enhancer could drive targeted gene expression in OHCs, the overall efficiency of gene delivery was lower than desired. This was evidenced by its failure to efficiently restore hearing function in Slc26a5 knockout mice. To address this limitation, we engineered B8, a synthetic enhancer with significantly improved efficiency, by dissecting and reconstructing key modules. B8-mediated delivery of Slc26a5 successfully restored the hearing sensitivity of Slc26a5 knockout mice. These results further underscore the utility of ARBITER in engineering enhancers with specific purposes and highlight the advantages of using cell-specific enhancers to treat hereditary hearing loss.

Our study also deepens our understanding of the fundamental principles governing enhancer-mediated gene expression. Although enhancers have been described for decades,[74,75] the basic principles of how individual elements within an enhancer cluster cooperate to mediate gene expression are not yet fully understood.[76,77] During our dissection of enhancers using ARBITER, we found that the collaborative interactions of enhancer modules are necessary to ensure the robust expression of target genes. For instance, the combined enhancer Slc26a5-E1 + E2 (SI-3) showed significantly improved transduction efficiency compared with individual elements alone. This observation was further confirmed in vivo by phenotype characterization of Slc26a5-E1 knockout and Slc26a5-E1 + E2 double knockout mice. The Slc26a5-E1 knockout resulted in progressive reduction in prestin expression during maturation, whereas the Slc26a5-E1 + E2 double knockout completely abolished the expression of prestin. Alongside previous findings showing that deletion of intron 2, which covered the sequence of Slc26a5-E2, led to delayed gene expression during OHC maturation,[59] these results revealed that the collaboration of two enhancer elements was essential to ensure the robust expression of target genes. Another interesting observation was that the enhancer Slc26a5-E1 did not activate target gene expression by itself but facilitated the gene expression level induced by Slc26a5-E2. These results revealed that this element might act as a transcriptional facilitator in gene regulation. Facilitators are a novel type of feature, identified during the analysis of the α-globin enhancer cluster, which lack classic enhancer activity but significantly improve the activity of classic enhancers.[78] Although some elements in the α-globin enhancer cluster exhibit characteristics of facilitators, controversy remains over whether facilitators are a common feature in enhancer clusters. The lack of the ability to extensively decode the features of each element in an

(H) Individual ABR and DPOAE thresholds across frequencies of gene-therapy-rescued mice from indicated groups. The bold line indicated the thresholds of mice with significant functional restoration after gene therapy. The denominator indicated the number in each group and the numerator indicated the number of mice with significant functional restoration.

(I) Representative SEM images of OHCs from Slc26a5^{+/+}, Slc26a5^{−/−}, and B8-Slc26a5 (5e10 gc) rescued mice. The white asterisks indicated the missing OHCs; the white arrows indicated the fused stereocilia bundles in Slc26a5^{−/−} mice. Scale bar, 2.5 μm. Data were shown as mean ± SEM. Group differences were analyzed by unpaired two-tailed t test. *$p < 0.05$, **$p < 0.01$, ***$p < 0.001$, #$p < 0.05$, ##$p < 0.01$, ###$p < 0.001$; NS, no significance.
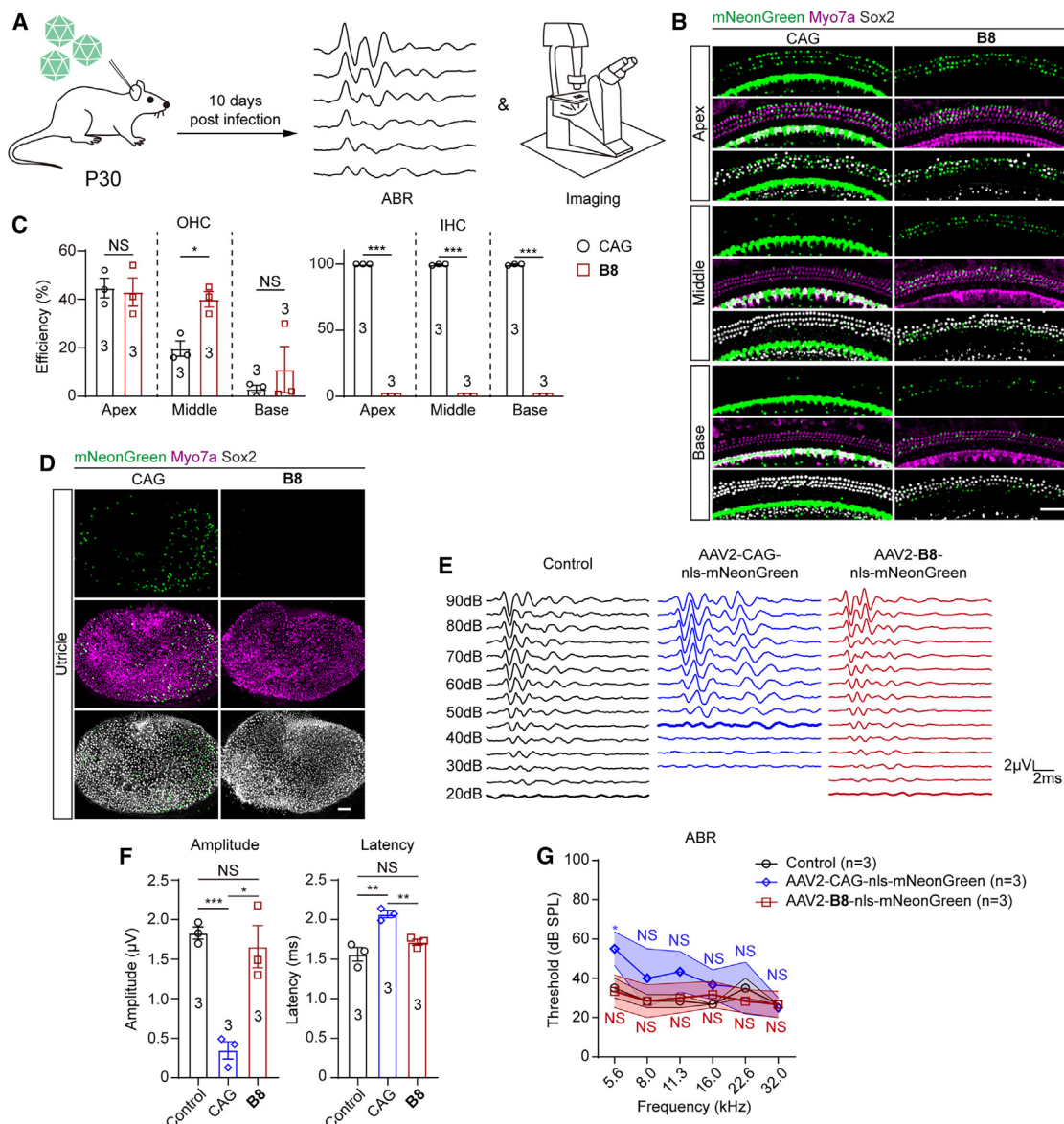
Figure 8. Safe and specific transduction of OHCs using B8 enhancer in adult mice

(A) Schematic illustration of experiment in adult mice. AAV2 reporters were delivered at P30 at a dose of 5e9 gc per mouse; functional tests and imaging experiments were performed at P40.

(B) Representative fluorescence images of infected cochlear cells in the apical, middle, and basal regions by CAG promoter and B8 enhancer.

(C) Quantification of the transduction efficiencies of CAG promoter and B8 enhancer on OHCs (left) and IHCs (right). *n* number in each group was labeled in the column.

(D) Representative fluorescence images of infected utricle cells by CAG promoter and B8 enhancer.

(E) Representative ABR waveforms at 16 kHz across all sound pressure levels; the bold line indicated the ABR thresholds.

(F) Statistics of peak amplitudes and latencies of ABR wave 1 evoked at 16 kHz by 90 dB SPL of mice from indicated group. *n* number in each group was labeled in the column.

(G) Comparisons of ABR thresholds across frequencies. *n* number in each group was labeled in the legend. Scale bar, 50 μm. Data were shown as mean ± SEM. *$p < 0.05$, **$p < 0.01$, ***$p < 0.001$; NS, no significance. Group differences were analyzed by unpaired two-tailed t test.

enhancer cluster highly limited the identification and analysis of facilitators. Here, ARBITER provided an efficient screening workflow for identifying facilitators, and our results indicated that facilitators may be a general principle to ensure robust activation of target genes.

RESOURCE AVAILABILITY

Lead contact

Further information and requests for resources and reagents should be directed to and will be fulfilled by the lead contact, Guisheng Zhong (zhongsh@shanghaitech.edu.cn).

Materials availability

Plasmids, mouse lines, and reagents generated in this study are available from the lead contact upon request.

Data and code availability

Data supporting the findings in this study are available within the paper and the supplemental information files, as well as upon reasonable request from the lead contact. This study did not generate original code.

AUTHOR CONTRIBUTIONS

G.Z. and S.Z. conceived the project and designed the experiments. S.Z. designed enhancers and reporters, and S.Z., Q.Y., and Y.X. constructed the plasmids. S.Z. and Q.Y. performed AAV packaging and purification. C.C. and S.D. performed AAV administration *in vivo*. Q.Y., C.C., Z.Y., L.F., S.D., and J.K. performed tissue dissection, cryo-section, and fluorescence staining. Q.Y. and M.D. performed confocal imaging. Z.Y. and Q.Y. performed ABR and DPOAE tests. Z.Y. performed SEM sample preparation and imaging. S.Z., Q.Y., M.D., L.F., Q.Z., and Y.L. processed confocal imaging data. C.C., H.L., Z.Y., and Y.-G.Y. performed tree shrew experiments. All the authors contributed to data analysis, interpretation, and presentation. G.Z., S.Z., Y.G.-Y., C.-P.L., and H.M. wrote the manuscript with contributions from all of the authors.

DECLARATION OF INTERESTS

C.C. is an employee and shareholder of Shanghai Emaygene Technology Co., Ltd. A patent related to this work has been submitted, the applicant is Shanghai Emaygene Technology Co., Ltd, and C.C. is listed as the inventor.

STAR★METHODS

Detailed methods are provided in the online version of this paper and include the following:

SUPPLEMENTAL INFORMATION

Supplemental information can be found online at https://doi.org/10.1016/j.neuron.2025.03.023.

REFERENCES

1. WHO. (2021). World Report on Hearing. https://www.who.int/publications/i/item/9789240020481.

2. Morton, C.C., and Nance, W.E. (2006). Newborn Hearing Screening — A Silent Revolution. N. Engl. J. Med. *354*, 2151–2164. https://doi.org/10.1056/NEJMra050700.

3. Angeli, S., Lin, X., and Liu, X.Z. (2012). Genetics of Hearing and Deafness. Anat. Rec. (Hoboken) *295*, 1812–1829. https://doi.org/10.1002/ar.22579.

4. Petit, C., Bonnet, C., and Safieddine, S. (2023). Deafness: from genetic architecture to gene therapy. Nat. Rev. Genet. *24*, 665–686. https://doi.org/10.1038/s41576-023-00597-7.

5. Müller, U., and Barr-Gillespie, P.G. (2015). New treatment options for hearing loss. Nat. Rev. Drug Discov. *14*, 346–365. https://doi.org/10.1038/nrd4533.

6. Jiang, L., Wang, D., He, Y., and Shu, Y. (2023). Advances in gene therapy hold promise for treating hereditary hearing loss. Mol. Ther. *31*, 934–950. https://doi.org/10.1016/j.ymthe.2023.02.001.

7. Lv, J., Wang, H., Cheng, X., Chen, Y., Wang, D., Zhang, L., Cao, Q., Tang, H., Hu, S., Gao, K., et al. (2024). AAV1-hOTOF gene therapy for autosomal recessive deafness 9: a single-arm trial. Lancet *403*, 2317–2325. https://doi.org/10.1016/S0140-6736(23)02874-X.

8. Wang, H., Chen, Y.X., Lv, J., Cheng, X.T., Cao, Q., Wang, D.Q., Zhang, L.L., Zhu, B.Y., Shen, M., Xu, C.X., et al. (2024). Bilateral gene therapy in children with autosomal recessive deafness 9: single-arm trial results. Nat. Med. *30*, 1898–1904. https://doi.org/10.1038/s41591-024-03023-5.

9. Qi, J., Tan, F., Zhang, L., Lu, L., Zhang, S., Zhai, Y., Lu, Y., Qian, X., Dong, W., Zhou, Y., et al. (2024). AAV-Mediated Gene Therapy Restores Hearing in Patients with DFNB9 Deafness. Adv. Sci. (Weinh) *11*, e2306788. https://doi.org/10.1002/advs.202306788.

10. Qi, J., Fu, X., Zhang, L., Tan, F., Li, N., Sun, Q., Hu, X., He, Z., Xia, M., and Chai, R. (2025). Current AAV-mediated gene therapy in sensorineural hearing loss. Fund. Res. *5*, 192–202. https://doi.org/10.1016/j.fmre.2022.08.015.

11. Li, C., and Samulski, R.J. (2020). Engineering adeno-associated virus vectors for gene therapy. Nat. Rev. Genet. *21*, 255–272. https://doi.org/10.1038/s41576-019-0205-4.

12. Food and Drug, Administration. (2021). Toxicity Risks of Adeno-associated Virus (AAV) Vectors for Gene Therapy. Cellular, Tissue, and Gene Therapies Advisory Committee (CTGTAC) Meeting #70 Briefing document. https://www.fda.gov/advisory-committees/cellular-tissue-and-gene-therapies-advisory-committee/meeting-materials-cellular-tissue-and-gene-therapies-advisory-committee.

13. Mullard, A. (2021). Gene therapy community grapples with toxicity issues, as pipeline matures. Nat. Rev. Drug Discov. *20*, 804–805. https://doi.org/10.1038/d41573-021-00164-x.

14. Donsante, A., Miller, D.G., Li, Y., Vogler, C., Brunt, E.M., Russell, D.W., and Sands, M.S. (2007). AAV Vector Integration Sites in Mouse Hepatocellular Carcinoma. Science *317*, 477. https://doi.org/10.1126/science.1142658.

15. Nguyen, G.N., Everett, J.K., Kafle, S., Roche, A.M., Raymond, H.E., Leiby, J., Wood, C., Assenmacher, C.-A., Merricks, E.P., Long, C.T., et al. (2021). A long-term study of AAV gene therapy in dogs with hemophilia A identifies clonal expansions of transduced liver cells. Nat. Biotechnol. *39*, 47–55. https://doi.org/10.1038/s41587-020-0741-7.

16. Venditti, C.P. (2021). Safety questions for AAV gene therapy. Nat. Biotechnol. *39*, 24–26. https://doi.org/10.1038/s41587-020-00756-9.

17. Caberlotto, E., Michel, V., Foucher, I., Bahloul, A., Goodyear, R.J., Pepermans, E., Michalski, N., Perfettini, I., Alegria-Prévot, O., Chardenoux, S., et al. (2011). Usher type 1G protein sans is a critical component of the tip-link complex, a structure controlling actin polymerization in stereocilia. Proc. Natl. Acad. Sci. USA *108*, 5825–5830. https://doi.org/10.1073/pnas.1017114108.

18. Zhang, L., Wang, H., Xun, M., Tang, H., Wang, J., Lv, J., Zhu, B., Chen, Y., Wang, D., Hu, S., et al. (2023). Preclinical evaluation of the efficacy and safety of AAV1-hOTOF in mice and nonhuman primates. Mol. Ther. Methods Clin. Dev. *31*, 101154. https://doi.org/10.1016/j.omtm.2023.101154.

19. Wang, H., Xun, M., Tang, H., Zhao, J., Hu, S., Zhang, L., Lv, J., Wang, D., Chen, Y., Liu, J., et al. (2024). Hair cell-specific Myo15 promoter-mediated gene therapy rescues hearing in DFNB9 mouse model. Mol. Ther. Nucleic Acids *35*, 102135. https://doi.org/10.1016/j.omtn.2024.102135.

20. Driver, E.C., and Kelley, M.W. (2020). Development of the cochlea. Development *147*, dev162263. https://doi.org/10.1242/dev.162263.

21. Roux, I., Safieddine, S., Nouvian, R., Grati, M.h., Simmler, M.-C., Bahloul, A., Perfettini, I., Le Gall, M., Rostaing, P., Hamard, G., et al. (2006). Otoferlin, Defective in a Human Deafness Form, Is Essential for Exocytosis at the Auditory Ribbon Synapse. Cell *127*, 277–289. https://doi.org/10.1016/j.cell.2006.08.040.

22. Seal, R.P., Akil, O., Yi, E., Weber, C.M., Grant, L., Yoo, J., Clause, A., Kandler, K., Noebels, J.L., Glowatzki, E., et al. (2008). Sensorineural Deafness and Seizures in Mice Lacking Vesicular Glutamate Transporter 3. Neuron *57*, 263–275. https://doi.org/10.1016/j.neuron.2007.11.032.

23. Zheng, J., Shen, W., He, D.Z.Z., Long, K.B., Madison, L.D., and Dallos, P. (2000). Prestin is the motor protein of cochlear outer hair cells. Nature *405*, 149–155. https://doi.org/10.1038/35012009.

24. Oliver, D., He, D.Z.Z., Klöcker, N., Ludwig, J., Schulte, U., Waldegger, S., Ruppersberg, J.P., Dallos, P., and Fakler, B. (2001). Intracellular Anions as the Voltage Sensor of Prestin, the Outer Hair Cell Motor Protein. Science *292*, 2340–2343. https://doi.org/10.1126/science.1060939.

25. Santos-Sacchi, J., Song, L., Zheng, J., and Nuttall, A.L. (2006). Control of Mammalian Cochlear Amplification by Chloride Anions. J. Neurosci. *26*, 3992–3998. https://doi.org/10.1523/JNEUROSCI.4548-05.2006.

26. Song, L., and Santos-Sacchi, J. (2013). Disparities in voltage-sensor charge and electromotility imply slow chloride-driven state transitions in the solute carrier SLC26a5. Proc. Natl. Acad. Sci. USA *110*, 3883–3888. https://doi.org/10.1073/pnas.1218341110.

27. Kurima, K., Peters, L.M., Yang, Y., Riazuddin, S., Ahmed, Z.M., Naz, S., Arnaud, D., Drury, S., Mo, J., Makishima, T., et al. (2002). Dominant and recessive deafness caused by mutations of a novel gene, TMC1, required for cochlear hair-cell function. Nat. Genet. *30*, 277–284. https://doi.org/10.1038/ng842.

28. Toms, M., Pagarkar, W., and Moosajee, M. (2020). Usher syndrome: clinical features, molecular genetics and advancing therapeutics. Ther. Adv. Ophthalmol. *12*, 2515841420952194. https://doi.org/10.1177/2515841420952194.

29. Bermingham, N.A., Hassan, B.A., Price, S.D., Vollrath, M.A., Ben-Arie, N., Eatock, R.A., Bellen, H.J., Lysakowski, A., and Zoghbi, H.Y. (1999). Math1: An Essential Gene for the Generation of Inner Ear Hair Cells. Science *284*, 1837–1841. https://doi.org/10.1126/science.284.5421.1837.

30. Zheng, J.L., and Gao, W.Q. (2000). Overexpression of Math1 induces robust production of extra hair cells in postnatal rat inner ears. Nat. Neurosci. *3*, 580–586. https://doi.org/10.1038/75753.

31. Wittkopp, P.J., and Kalay, G. (2011). Cis-regulatory elements: molecular mechanisms and evolutionary processes underlying divergence. Nat. Rev. Genet. *13*, 59–69. https://doi.org/10.1038/nrg3095.

32. de Laat, W., and Duboule, D. (2013). Topology of mammalian developmental enhancers and their regulatory landscapes. Nature *502*, 499–506. https://doi.org/10.1038/nature12753.

33. Claringbould, A., and Zaugg, J.B. (2021). Enhancers in disease: molecular basis and emerging treatment strategies. Trends Mol. Med. *27*, 1060–1073. https://doi.org/10.1016/j.molmed.2021.07.012.

34. Barski, A., Cuddapah, S., Cui, K., Roh, T.-Y., Schones, D.E., Wang, Z., Wei, G., Chepelev, I., and Zhao, K. (2007). High-Resolution Profiling of Histone Methylations in the Human Genome. Cell *129*, 823–837. https://doi.org/10.1016/j.cell.2007.05.009.

35. Buenrostro, J.D., Giresi, P.G., Zaba, L.C., Chang, H.Y., and Greenleaf, W.J. (2013). Transposition of native chromatin for fast and sensitive epigenomic profiling of open chromatin, DNA-binding proteins and nucleosome position. Nat. Methods *10*, 1213–1218. https://doi.org/10.1038/nmeth.2688.

36. Fulco, C.P., Munschauer, M., Anyoha, R., Munson, G., Grossman, S.R., Perez, E.M., Kane, M., Cleary, B., Lander, E.S., and Engreitz, J.M. (2016). Systematic mapping of functional enhancer–promoter connections with CRISPR interference. Science *354*, 769–773. https://doi.org/10.1126/science.aag2445.

37. Klann, T.S., Black, J.B., Chellappan, M., Safi, A., Song, L., Hilton, I.B., Crawford, G.E., Reddy, T.E., and Gersbach, C.A. (2017). CRISPR–Cas9 epigenome editing enables high-throughput screening for functional regulatory elements in the human genome. Nat. Biotechnol. *35*, 561–568. https://doi.org/10.1038/nbt.3853.

38. Gasperini, M., Hill, A.J., McFaline-Figueroa, J.L., Martin, B., Kim, S., Zhang, M.D., Jackson, D., Leith, A., Schreiber, J., Noble, W.S., et al. (2019). A Genome-wide Framework for Mapping Gene Regulation via Cellular Genetic Screens. Cell *176*, 377–390.e19. https://doi.org/10.1016/j.cell.2018.11.029.

39. Luo, Z., Du, Y., Li, S., Zhang, H., Shu, M., Zhang, D., He, S., Wang, G., Lu, F., and Liu, Z. (2022). Three distinct Atoh1 enhancers cooperate for sound receptor hair cell development. Proc. Natl. Acad. Sci. USA *119*, e2119850119. https://doi.org/10.1073/pnas.2119850119.

40. Tao, L., Yu, H.V., Llamas, J., Trecek, T., Wang, X., Stojanova, Z., Groves, A.K., and Segil, N. (2021). Enhancer decommissioning imposes an epigenetic barrier to sensory hair cell regeneration. Dev. Cell *56*, 2471–2485.e5. https://doi.org/10.1016/j.devcel.2021.07.003.

41. Iyer, A.A., Hosamani, I., Nguyen, J.D., Cai, T., Singh, S., McGovern, M.M., Beyer, L., Zhang, H., Jen, H.-I., Yousaf, R., et al. (2022). Cellular reprogramming with ATOH1, GFI1, and POU4F3 implicate epigenetic changes and cell-cell signaling as obstacles to hair cell regeneration in mature mammals. eLife *11*, e79712. https://doi.org/10.7554/eLife.79712.

42. Tan, F., Chu, C., Qi, J., Li, W., You, D., Li, K., Chen, X., Zhao, W., Cheng, C., Liu, X., et al. (2019). AAV-ie enables safe and efficient gene transfer to inner ear cells. Nat. Commun. *10*, 3733. https://doi.org/10.1038/s41467-019-11687-8.

43. Bejerano, G., Pheasant, M., Makunin, I., Stephen, S., Kent, W.J., Mattick, J.S., and Haussler, D. (2004). Ultraconserved Elements in the Human Genome. Science *304*, 1321–1325. https://doi.org/10.1126/science.1098119.

44. Dickel, D.E., Ypsilanti, A.R., Pla, R., Zhu, Y., Barozzi, I., Mannion, B.J., Khin, Y.S., Fukuda-Yuzawa, Y., Plajzer-Frick, I., Pickle, C.S., et al. (2018). Ultraconserved Enhancers Are Required for Normal Development. Cell *172*, 491–499.e415. https://doi.org/10.1016/j.cell.2017.12.017.

45. Pennacchio, L.A., Ahituv, N., Moses, A.M., Prabhakar, S., Nobrega, M.A., Shoukry, M., Minovitsky, S., Dubchak, I., Holt, A., Lewis, K.D., et al. (2006).

In vivo enhancer analysis of human conserved non-coding sequences. Nature *444*, 499–502. https://doi.org/10.1038/nature05295.

46. Visel, A., Prabhakar, S., Akiyama, J.A., Shoukry, M., Lewis, K.D., Holt, A., Plajzer-Frick, I., Afzal, V., Rubin, E.M., and Pennacchio, L.A. (2008). Ultraconservation identifies a small subset of extremely constrained developmental enhancers. Nat. Genet. *40*, 158–160. https://doi.org/10.1038/ng.2007.55.

47. Kent, W.J., Sugnet, C.W., Furey, T.S., Roskin, K.M., Pringle, T.H., Zahler, A.M., and Haussler, D. (2002). The Human Genome Browser at UCSC. Genome Res. *12*, 996–1006. https://doi.org/10.1101/gr.229102.

48. Perez, G., Barber, G.P., Benet-Pages, A., Casper, J., Clawson, H., Diekhans, M., Fischer, C., Gonzalez, J.N., Hinrichs, A.S., Lee, C.M., et al. (2025). The UCSC Genome Browser database: 2025 update. Nucleic Acids Res. *53*, D1243–D1249. https://doi.org/10.1093/nar/gkae974.

49. Hansen, J., Mailand, E., Swaminathan, K.K., Schreiber, J., Angelici, B., and Benenson, Y. (2014). Transplantation of prokaryotic two-component signaling pathways into mammalian cells. Proc. Natl. Acad. Sci. USA *111*, 15705–15710. https://doi.org/10.1073/pnas.1406482111.

50. Ede, C., Chen, X., Lin, M.-Y., and Chen, Y.Y. (2016). Quantitative Analyses of Core Promoters Enable Precise Engineering of Regulated Gene Expression in Mammalian Cells. ACS Synth. Biol. *5*, 395–404. https://doi.org/10.1021/acssynbio.5b00266.

51. Li, S., Fan, T., Li, C., Wang, Y., Li, J., and Liu, Z. (2022). Fate-mapping analysis of cochlear cells expressing Atoh1 mRNA via a new Atoh1$^{3*HA-P2A-Cre}$ knockin mouse strain. Dev. Dyn. *251*, 1156–1174. https://doi.org/10.1002/dvdy.453.

52. Yao, Y.-G., Lu, L., Ni, R.-J., Bi, R., Chen, C., Chen, J.-Q., Fuchs, E., Gorbatyuk, M., Lei, H., Li, H., et al. (2024). Study of tree shrew biology and models: A booming and prosperous field for biomedical research. Zool. Res. *45*, 877–909. https://doi.org/10.24272/j.issn.2095-8137.2024.199.

53. Ye, M.-S., Zhang, J.-Y., Yu, D.-D., Xu, M., Xu, L., Lv, L.-B., Zhu, Q.-Y., Fan, Y., and Yao, Y.-G. (2021). Comprehensive annotation of the Chinese tree shrew genome by large-scale RNA sequencing and long-read isoform sequencing. Zool. Res. *42*, 692–709. https://doi.org/10.24272/j.issn.2095-8137.2021.272.

54. Xiao, J., Liu, R., and Chen, C.-S. (2017). Tree shrew (*Tupaia belangeri*) as a novel laboratory disease animal model. Zool. Res. *38*, 127–137. https://doi.org/10.24272/j.issn.2095-8137.2017.033.

55. Jiang, J.-H., Wang, Y.-F., Zheng, J., Lei, Y.-M., Chen, Z.-Y., Guo, Y., Guo, Y.-J., Guo, B.-Q., Lv, Y.-F., Wang, H.-H., et al. (2024). Human-like adrenal features in Chinese tree shrews revealed by multi-omics analysis of adrenal cell populations and steroid synthesis. Zool. Res. *45*, 617–632. https://doi.org/10.24272/j.issn.2095-8137.2023.280.

56. Lihong, X., Heng, L., Gyanwali, B., Meichan, Z., Kaiquan, Z., Kai, S., and Anzhou, T. (2016). Micro-computed tomography and microdissection of the temporal bone of tree shrews. Ann. Anat. *208*, 69–77. https://doi.org/10.1016/j.aanat.2015.08.005.

57. Biedron, S., Westhofen, M., and Ilgner, J. (2009). On the Number of Turns in Human Cochleae. Otol. Neurotol. *30*, 414–417. https://doi.org/10.1097/MAO.0b013e3181977b8d.

58. Yamashita, T., Hakizimana, P., Wu, S., Hassan, A., Jacob, S., Temirov, J., Fang, J., Mellado-Lagarde, M., Gursky, R., Horner, L., et al. (2015). Outer Hair Cell Lateral Wall Structure Constrains the Mobility of Plasma Membrane Proteins. PLoS Genet. *11*, e1005500. https://doi.org/10.1371/journal.pgen.1005500.

59. Sun, Y., Zhang, Y., Zhang, D., Wang, G., Song, L., and Liu, Z. (2022). In vivo CRISPR-Cas9-mediated DNA chop identifies a cochlear outer hair cell-specific enhancer. FASEB J. *36*, e22233. https://doi.org/10.1096/fj.202100421RR.

60. Sheffield, A.M., and Smith, R.J.H. (2019). The Epidemiology of Deafness. Cold Spring Harb. Perspect. Med. *9*, a033258. https://doi.org/10.1101/cshperspect.a033258.

61. Zhang, H., Pan, H., Zhou, C., Wei, Y., Ying, W., Li, S., Wang, G., Li, C., Ren, Y., Li, G., et al. (2018). Simultaneous zygotic inactivation of multiple genes in mouse through CRISPR/Cas9-mediated base editing. Development *145*, dev168906. https://doi.org/10.1242/dev.168906.

62. Tao, Y., Liu, X., Yang, L., Chu, C., Tan, F., Yu, Z., Ke, J., Li, X., Zheng, X., Zhao, X., et al. (2022). AAV-ie-K558R mediated cochlear gene therapy and hair cell regeneration. Signal Transduct. Target. Ther. *7*, 109. https://doi.org/10.1038/s41392-022-00938-8.

63. Zhu, W., Du, W., Rameshbabu, A.P., Armstrong, A.M., Silver, S., Kim, Y., Wei, W., Shu, Y., Liu, X., Lewis, M.A., et al. (2024). Targeted genome editing restores auditory function in adult mice with progressive hearing loss caused by a human microRNA mutation. Sci. Transl. Med. *16*, eadn0689. https://doi.org/10.1126/scitranslmed.adn0689.

64. Omichi, R., Yoshimura, H., Shibata, S.B., Vandenberghe, L.H., and Smith, R.J.H. (2020). Hair Cell Transduction Efficiency of Single- and Dual-AAV Serotypes in Adult Murine Cochleae. Mol. Ther. Methods Clin. Dev. *17*, 1167–1177. https://doi.org/10.1016/j.omtm.2020.05.007.

65. Lesica, N.A. (2018). Why Do Hearing Aids Fail to Restore Normal Auditory Perception? Trends Neurosci. *41*, 174–185. https://doi.org/10.1016/j.tins.2018.01.008.

66. Landegger, L.D., Pan, B., Askew, C., Wassmer, S.J., Gluck, S.D., Galvin, A., Taylor, R., Forge, A., Stankovic, K.M., Holt, J.R., et al. (2017). A synthetic AAV vector enables safe and efficient gene transfer to the mammalian inner ear. Nat. Biotechnol. *35*, 280–284. https://doi.org/10.1038/nbt.3781.

67. Isgrig, K., McDougald, D.S., Zhu, J., Wang, H.J., Bennett, J., and Chien, W.W. (2019). AAV2.7m8 is a powerful viral vector for inner ear gene therapy. Nat. Commun. *10*, 427. https://doi.org/10.1038/s41467-018-08243-1.

68. Lee, J., Nist-Lund, C., Solanes, P., Goldberg, H., Wu, J., Pan, B., Schneider, B.L., and Holt, J.R. (2020). Efficient viral transduction in mouse inner ear hair cells with utricle injection and AAV9-PHP.B. Hear. Res. *394*, 107882. https://doi.org/10.1016/j.heares.2020.107882.

69. Artemyev, V., Gubaeva, A., Paremskaia, A.I., Dzhioeva, A.A., Deviatkin, A., Feoktistova, S.G., Mityaeva, O., and Volchkov, P.Y. (2024). Synthetic Promoters in Gene Therapy: Design Approaches, Features and Applications. Cells *13*, 1963. https://doi.org/10.3390/cells13231963.

70. Ye, G.-J., Budzynski, E., Sonnentag, P., Nork, T.M., Sheibani, N., Gurel, Z., Boye, S.L., Peterson, J.J., Boye, S.E., Hauswirth, W.W., et al. (2016). Cone-Specific Promoters for Gene Therapy of Achromatopsia and Other Retinal Diseases. Hum. Gene Ther. *27*, 72–82. https://doi.org/10.1089/hum.2015.130.

71. Tabebordbar, M., Lagerborg, K.A., Stanton, A., King, E.M., Ye, S., Tellez, L., Krunnfusz, A., Tavakoli, S., Widrick, J.J., Messemer, K.A., et al. (2021). Directed evolution of a family of AAV capsid variants enabling potent muscle-directed gene delivery across species. Cell *184*, 4919–4938.e22. https://doi.org/10.1016/j.cell.2021.08.028.

72. Rajarajan, P., Gil, S.E., Brennand, K.J., and Akbarian, S. (2016). Spatial genome organization and cognition. Nat. Rev. Neurosci. *17*, 681–691. https://doi.org/10.1038/nrn.2016.124.

73. Hafner, A., and Boettiger, A. (2023). The spatial organization of transcriptional control. Nat. Rev. Genet. *24*, 53–68. https://doi.org/10.1038/s41576-022-00526-0.

74. Banerji, J., Rusconi, S., and Schaffner, W. (1981). Expression of a β-globin gene is enhanced by remote SV40 DNA sequences. Cell *27*, 299–308. https://doi.org/10.1016/0092-8674(81)90413-X.

75. Mercola, M., Wang, X.F., Olsen, J., and Calame, K. (1983). Transcriptional Enhancer Elements in the Mouse Immunoglobulin Heavy Chain Locus. Science *221*, 663–665. https://doi.org/10.1126/science.6306772.

76. Osterwalder, M., Barozzi, I., Tissières, V., Fukuda-Yuzawa, Y., Mannion, B.J., Afzal, S.Y., Lee, E.A., Zhu, Y., Plajzer-Frick, I., Pickle, C.S., et al. (2018). Enhancer redundancy provides phenotypic robustness in mammalian development. Nature *554*, 239–243. https://doi.org/10.1038/nature25461.

77. Kvon, E.Z., Waymack, R., Gad, M., and Wunderlich, Z. (2021). Enhancer redundancy in development and disease. Nat. Rev. Genet. *22*, 324–336. https://doi.org/10.1038/s41576-020-00311-x.

78. Blayney, J.W., Francis, H., Rampasekova, A., Camellato, B., Mitchell, L., Stolper, R., Cornell, L., Babbs, C., Boeke, J.D., Higgs, D.R., et al. (2023). Super-enhancers include classical enhancers and facilitators to fully activate gene expression. Cell *186*, 5826–5839.e18. https://doi.org/10.1016/j.cell.2023.11.030.

79. Chen, S., Zhou, Y., Chen, Y., and Gu, J. (2018). fastp: an ultra-fast all-in-one FASTQ preprocessor. Bioinformatics *34*, i884–i890. https://doi.org/10.1093/bioinformatics/bty560.

80. Langmead, B., and Salzberg, S.L. (2012). Fast gapped-read alignment with Bowtie 2. Nat. Methods *9*, 357–359. https://doi.org/10.1038/nmeth.1923.

81. Li, H., Handsaker, B., Wysoker, A., Fennell, T., Ruan, J., Homer, N., Marth, G., Abecasis, G., and Durbin, R.; 1000 Genome Project Data Processing Subgroup (2009). The Sequence Alignment/Map format and SAMtools. Bioinformatics *25*, 2078–2079. https://doi.org/10.1093/bioinformatics/btp352.

82. Chen, J.-Q., Zhang, Q., Yu, D., Bi, R., Ma, Y., Li, Y., Lv, L.-B., and Yao, Y.-G. (2022). Optimization of Milk Substitutes for the Artificial Rearing of Chinese Tree Shrews (Tupaia belangeri chinensis). Animals (Basel) *12*, 1655. https://doi.org/10.3390/ani12131655.

STAR★METHODS

KEY RESOURCES TABLE

REAGENT or RESOURCE	SOURCE	IDENTIFIER
Antibodies		
Rabbit polyclonal anti-myosin 7A antibody	Proteus Biosciences	Cat# 25-6790; RRID: AB_10015251
Goat polyclonal anti-Sox2 antibody	R&D Systems	Cat# AF2018; RRID:AB_355110
Goat polyclonal anti-Prestin antibody	Santa Cruz Biotechnology	Cat# sc-22692; RRID:AB_2302038
Bacterial and virus strains		
AAV reporter vectors carrying different synthetic enhancers	This paper, see Table S2	N/A
AAV-ie-CAG-*Slc26a5*	This paper	N/A
AAV-ie-*Slc26a5*-E1+E2-*Slc26a5*	This paper	N/A
AAV-ie-**B8**-*Slc26a5*	This paper	N/A
AAV2-CAG-nls-mNeonGreen	This paper	N/A
AAV2-**B8**-nls-mNeonGreen	This paper	N/A
Biological samples		
Mouse cochlear sample	This paper	N/A
Mouse vestibular sample	This paper	N/A
Mouse brain	This paper	N/A
Tree shew cochlear sample	This paper	N/A
Tree shew vestibular sample	This paper	N/A
Chemicals, peptides, and recombinant proteins		
DMEM cell culture medium	EpiZyme	Cat# CB001
Fetal bovine serum (FBS)	Excell	Cat# FSP500
Penicillin/streptomycin solution	EpiZyme	Cat# CB010
0.05% Trypsin	Coolaber	Cat# SL6013
PEG8000	Yeasen	Cat# 60304ES76
NaCl	ABCONE	Cat# S39168
Pluronic F68	ThermoFisher	Cat# 24040032
MgCl$_2$	HUSHI	Cat# 10012818
DNase I	Thermo Fisher	Cat# EN0521
RNase A	Tiangen	Cat# RT405
Iodixanol solution	Sigma-Aldrich	Cat# D1556
Zoletil®50	Virbac	N/A
Dermafuse™ issue adhesive	Millpledge	N/A
Paraformaldehyde (PFA)	Sbjbio	Cat# BL-G002
EDTA	ABCONE	Cat# E27918
DAPI	Beyotime	Cat# C1002
Osmium tetroxide	Ted Pella, Inc	Cat#18465
Tannic acid	Sigma-Aldrich	Cat#V900190
Conductive silver	SPI Supplies	Cat#1250115
Mounting media	Vectorlabs	Cat# H1200-10
Critical commercial assays		
Phanta MaxSuper-Fidelity DNA Polymerase	Vazyme	Cat# P505
Fastdigest XbaI	Thermo Fisher	Cat# FD0684
Fastdigest KpnI	Thermo Fisher	Cat# FD0524
One-Step PCR Cloning Kit	Novoprotein	Cat# NR005-01B
ChamQ Universal SYBR qPCR Master Mix	Vazyme	Cat# Q711

(Continued on next page)

Continued

REAGENT or RESOURCE	SOURCE	IDENTIFIER
Experimental models: Cell lines		
HEK-293T	ATCC	Cat# CRL-3216
Experimental models: Organisms/strains		
C57BL/6 wildtype mice	Lingchang Biotech Co., Ltd	N/A
Slc26a5 knockout mice	a kindly gift from Prof. Zhiyong Liu lab[61]	N/A
Slc26a5-E1 knockout mice	This paper	N/A
Slc26a5-E1+E2 double knockout mice	This paper	N/A
Tree shrew model	This paper	N/A
Oligonucleotides		
Primers for genotyping	This paper, see Table S1	N/A
Guide RNA-1 for *Slc26a5*-E1 deletion: CTGGACTATGGAGAGTGCCG	This paper	N/A
Guide RNA-2 for *Slc26a5*-E1 deletion: GCTTTGCTCGTTGCTATCAT	This paper	N/A
Guide RNA-3 for *Slc26a5*-E2 deletion: AGCAGCCCCACGCTCACCAA	This paper	N/A
Guide RNA-4 for *Slc26a5*-E2 deletion: GCTTTGCTCGTTGCTATCAT	This paper	N/A
qPCR primer WPRE-F: AGTGTAGATAGTAGACTGTC	This paper	N/A
qPCR primer WPRE-R: GGCGATGAGTTCCGCCGTGGC	This paper	N/A
Recombinant DNA		
pAAV plasmids carrying synthetic enhancers in this paper	This paper, custom design and in-house cloning, see also Table S2	N/A
pAAV-CAG-*Slc26a5*	This paper	N/A
pAAV-*Slc26a5*-E1+E2-*Slc26a5*	This paper	N/A
pAAV-**B8**-*Slc26a5*	This paper	N/A
pAAV-CAG-nls-mNeonGreen	In-house cloning[42]	N/A
pHelper	In-house cloning[42]	N/A
pRep2-CapIE	In-house cloning[42]	N/A
pRep2-Cap2	In-house cloning[42]	N/A
Software and algorithms		
FIJI software	ImageJ	imagej.github.io/imagej-wiki-static/Install_Fiji_on_Windows
BioSigRP software	Tucker-Davis Technology	N/A
GraphPad Prism 8.0	Graphpad software	https://www.graphpad.com/scientific-software/prism/
Fastp	Chen et al.[79]	https://github.com/OpenGene/fastp
Bowtie2	Langmead and Salzberg[80]	https://github.com/BenLangmead/bowtie2
SAMtools	Li et al.[81]	https://github.com/samtools/samtools
Other		
Ultra-15 centrifugal filter units	Amicon Ultra	Cat# UFC910024
Tucker-Davis Technology System III	Tucker-Davies Technologies	N/A
Field-emission scanning electron microscope	Zeiss	GeminiSEM 460
Critical point dryer	Leica	EM CPD300
Vaccum Coater	Leica	EM ACE200
Microtome	Leica	CM1950
Confocal microscope	Nikon	A1R
Spinning disc microscope	Nikon	SORA

EXPERIMENTAL MODEL AND STUDY PARTICIPANT DETAILS

Animal models

Mouse and tree shrew models were used in this study, and the animal experiments were performed in accordance with standard ethical guidelines and approved by the IACUC of ShanghaiTech University (mouse study) and Kunming Institute of Zoology, Chinese Academy of Sciences (tree shrew study), China. Efforts were made to minimize the number of animals used and their suffering. The number of days since birth was counted from post-natal day 0 (P0). Mice were housed under a 12 h light/dark cycle at a room temperature with food and water available *ad libitum*. Wild-type C57BL/6 mice, *Slc26a5*-E1 knockout (*Slc26a5*-E1$^{-/-}$E2$^{+/+}$), *Slc26a5*-E1+E2 double knockout (*Slc26a5*-E1$^{-/-}$E2$^{-/-}$), and Slc26a5$^{-/-}$ mouse strains were used in this study. Wild-type C57BL/6 mice were purchased from Shanghai Lingchang Biotech Co., Ltd. (Shanghai, China).

The *Slc26a5*-E1 knockout and *Slc26a5*-E1+E2 double knockout mouse strain were generated at Gempharmatech Co., Ltd. (Nanjing, China). The *Slc26a5*-E1 sequence within intron 1 of the *Slc26a5* gene was deleted by using the CRISPR-Cas9 system. Due to the convenience of sgRNA design, a sequence of 578 bps has been excised. sgRNAs targeting the upstream and downstream of *Slc26a5*-E1 (sgRNA1: CTGGACTATGGAGAGTGCCG; sgRNA2: GCTTTGCTCGTTGCTATCAT) were designed and injected into one-cell stage zygotes together with the CRISPR-Cas9 protein, followed by implantation into pseudopregnant female mice. Obtained F0 mice were genotyped by tail PCR, and Sanger sequencing were performed to confirm the deletion of *Slc26a5*-E1. Positive pups in the F0 progeny were crossed with the wild-type mice in a C57BL/6 background. To generate *Slc26a5*-E1+E2 double knockout mice, *Slc26a5*-E1 knockout mouse strain was used as the background. sgRNAs targeting the upstream and downstream of *Slc26a5*-E2 (sgRNA3: AGCAGCCCCACGCTCACCAA; sgRNA4: AGTGTAGATAGTAGACTGTC) were designed and co-injected with the CRISPR-Cas9 protein into one-cell stage zygotes of *Slc26a5*-E1 knockout mice, followed by implantation into pseudopregnant female mice. Obtained F0 mice were genotyped by tail PCR, and Sanger sequencing were performed to confirm the deletion of *Slc26a5*-E1 and E2. Positive pups in the F0 progeny were further crossed with the wild-type mice in a C57BL/6 background. For routine genotype analysis of F1 or later mouse progeny, genotyping was performed using PCR primers detailed in Table S1.

The Slc26a5$^{-/-}$ mouse strain was generously provided by Prof. Zhiyong Liu as a gift and was generated using CRISPR/Cas9-mediated base editing strategy.[61] For routine genotype analysis of F1 or later mouse progeny, PCR was performed on mouse tail DNA. The PCR amplicon underwent Sanger sequencing, and the sequencing analysis were used to assess whether the codons had mutated into stop codons. The PCR primers were listed in Table S1.

A female tree shrew aging 4-month old was chosen from the breeding colonies[82] of the Experimental Animal Center of the Kunming Institute of Zoology, Chinese Academy of Sciences. Animals were individually housed in a fully acclimatized facility with access to food twice daily and water *ad libitum* under a 12 h inverted day/night cycle (lights on at 7:00 am and lights off at 7:00 pm). All tree shrews had normal weight and behavior during the experiments.

Cell lines

HEK293T cells were maintained using DMEM medium supplemented with 10% fetal bovine serum (FBS), and penicillin/streptomycin.

METHOD DETAILS

Enhancer design and construction

The sequences of *Atoh1* enhancers were selected based on previous published ATAC-seq data (GSE181311). Data analysis was performed as previously described.[39] Briefly, the reads were trimmed with fastp[79] with default parameters, and aligned to GRCm39/mm39 genome assembly with Bowtie2.[80] Mapped reads were further sorted using SAMtools.[81] Elements within 2−200 kb upstream or downstream of *Atoh1* TSS were considered as potential regulatory elements. The CNEs within the gene loci of *Slc26a5* and *Myo7a* were analyzed utilizing the Phylop score track in UCSC Genome Browser (https://genome.ucsc.edu/).[47,48] Sequences with Phylop scores surpassing 1.0 were defined as conserved sequences. The region from 50 kb upstream of TSS to 50 kb downstream of the last exon was considered as the gene locus. Conserved noncoding sequences longer than 100 bp within this region were selected as candidate CNEs for further validation.

The selected sequences were amplified via PCR from the mouse or human genome using Phanta MaxSuper-Fidelity DNA Polymerase, and subsequently cloned into an pAAV reporter plasmid, with a synthetic minimal promoter (MinP: TAGAGGGTATATAA TGGAAGCTCGACTTCCAG) fused downstream to initiate the basal gene expression. The pAAV reporter plasmids were generated based on a pAAV-CAG-NLS-mNeonGreen plasmid, which encapsulates the CAG promoter, nuclear localization sequence (NLS), the fluorescent protein mNeonGreen, the WPRE element, as well as the SV40 polyA sequence.[42] The pAAV-CAG-NLS-mNeonGreen plasmid was cleaved using restriction endonuclease *Xba*I and *Kpn*I for linearization, and the candidate elements were incorporated into this vector through homologous recombination, employing the One-Step PCR Cloning Kit.

Evolutionary conservation analysis and sequence segmentation

The conservation of the elements was analyzed using Align function in Uniprot (https://www.uniprot.org/align). Sequences derived from mouse (*Mus musculus*), rat (*Rattus norvegicus*), tree shrew (*Tupaia belangeri*), human (*Homo sapiens*), rhesus (*Macaca mulatta*), marmoset (*Callithrix jacchus*), dog (*Canis lupus familiaris*), pig (*Sus scrofa*), and rabbit (*Oryctolagus cuniculus*) were downloaded from

GenBank and aligned, and the sequence identities across species were used to represent the conservation. For the sequence segmentation assay, *Slc26a5*-E1 was divided into three parts based on the length and conservation, and *Slc26a5*-E2 was separated into four parts accordingly. Each part was further analyzed for their conservation using alignment. When calculating the correlations between the transduction efficiency or intensity and sequence conservation of the segments, the average sequence identity of each segment between mouse and other eight selected species was used to represent the conservation accordingly.

AAV package and purification

All AAVs were generated by the traditional co-transfection of three plasmids in HEK293T cells. When HEK293T cells reached 80-90% confluence, a 150 mm diameter cell culture dish was subjected to co-transfection using the calcium phosphate transfection method with an AAV transgene plasmid, a rep-cap fused plasmid, and a helper plasmid. The culture medium was replenished 8 hours after transfection with medium containing 1% FBS. After a 48 h post-transfection period, the cultured supernatant was harvested, and the medium was substituted with DMEM supplemented with 1% FBS. Both the culture medium and cells were harvested 96 h post-transfection. Supernatant and cells were subjected to chloroform treatment at 37 $^{\circ}$C for 1 hour to induce cell lysis and eliminate unwanted proteins. After high-speed centrifugation at 36,000 ×g at 4 $^{\circ}$C, the combined medium and supernatant were precipitated and concentrated overnight at 4°C using 10% PEG8000 and 1M NaCl. After centrifugation at 60,000 ×g for 20 minutes, the precipitates were suspended in the digestion buffer containing PBS buffer, 0.001% Pluronic F68, 2.5 mM MgCl$_2$, 1U/μL DNase I and 0.1μg/μL RNase A. The precipitates were subjected to digestion to eliminate other DNA and RNA, conducted at 37 $^{\circ}$C overnight. The crude AAV stocks were further purified over iodixanol step gradients (15%, 25%, 40%, 60%). Following ultracentrifugation in a 70Ti rotor for 2 hours and 25 minutes at 200,000 ×g at 18 $^{\circ}$C, and the 40% fraction containing AAVs was collected. Iodixanol was removed and replaced with PBS buffer containing 0.001% pluronic F68, followed by the concentration of AAVs using Ultra-15 centrifugal filter units.

The quantification of purified AAVs was performed using SYBR qPCR analysis with the qPCR primers targeting the WPRE region.

AAV administration

The surgical site was aseptically prepared by wiping with 75% ethanol. Surgery was exclusively conducted on the right ear of each animal, with the left ear serving as a negative control.

For neonatal mouse injections, we followed a surgical procedure outlined in the literature known as round window membrane (RWM) injection.[42,66] Briefly, the neonatal mice were anesthetized by exposure to low temperatures for 2-3 min on ice. The RWM was punctured using a glass electrode, and the injected volume was maintained at approximately 1 μL per ear. Following the injection, the skin incision was closed using veterinary tissue adhesive (Millpledge). After the surgery, pups were rewarmed on a 37 $^{\circ}$C heating pad for 10-15 min and then returned to the parental cage.

For injections in adult mice and tree shrews, we conducted posterior semicircular canal (PSCC) injections. After the animals were anesthetized with Zoletil®50 (60 mg/kg, 0.2% Xylazine), the depilated hair was wiped away with a cotton swab, exposing the skin of the surgical area. A 37 $^{\circ}$C heating pad was placed under the microscope to maintain the animal's body temperature during the surgery. The skin was gently incised with surgical scissors below the ear canal, creating a wound approximately 0.5-1 cm in length. Subcutaneous fat was gently dissected with surgical forceps to expose the muscle. After exposing PSCC, surrounding muscles were cleared to ensure an adequate surgical area. A straight hook was used to drill a small hole on the PSCC. After lymphatic fluid drainage, any remaining lymphatic fluid was absorbed with a cotton swab. AAVs were injected into the PSCC through a glass electrode. After injection, the glass electrode was gently withdrawn, adhered to the opening of the PSCC using veterinary tissue adhesive, sealing the wound to prevent lymphatic fluid and virus leakage. The wound was gently sealed using veterinary tissue adhesive. After the surgery, animals were placed on a 37 $^{\circ}$C heating pad, allowed to recover, and then returned to the cage for continued care.

Immunofluorescence labeling

Animals were anesthetized and transcardially perfused with 0.1 M PBS buffer (pH 7.4) at room temperature and then with freshly prepared, ice-cold 4% paraformaldehyde (PFA) in PBS. The temporal bones were harvested and post-fixed in 4% PFA in PBS (pH 7.2) for 2 h at room temperature. Following treatment with 0.5 mM EDTA (pH 8.0) for 0.5-6 h, the cochleae and vestibular tissues were dissected for immunostaining. For cross-section of the cochlea, cochleae were excised and fixed in 4% PFA for 2 h, followed by decalcification in 0.5 M EDTA at room temperature for 2 h. Specimens were cryo-protected in 30% sucrose in PBS and then embedded in optimal cutting temperature (OCT) compound, frozen, and sectioned (14 μm). For cross section of the brain, the heart, and the liver, tissues were post-fixed in 4% PFA overnight and then treated with a sucrose gradient (10–30% in PBS). After freezing at -80 $^{\circ}$C, the tissues were cross-sectioned at 10-20 μm thickness.

Samples were permeabilized and blocked in the blocking buffer (10% donkey serum in 0.3% Triton X-100 in PBS) for 1 h at room temperature, and then subsequently stained with antibodies against myosin 7A, Sox2 together with corresponding secondary antibodies. Samples were mounted with anti-fluorescence quenching agent Vectorshield with DAPI mounting media.

Confocal imaging

Mounted samples were imaged with Nikon inverted confocal microscope or Nikon spinning disc microscope. Z stacks with optical sections of 1.0 μm intervals were collected using a 20× objective lens and NIS-Elements Viewer. The transduction efficiency and

protein expression levels were analyzed using ImageJ FIJI software. Transduction efficiency was defined as percentage of reporter positive cell populations.

Reporter intensity normalization

For reliable quantification and comparison of AAV reporter expression levels, particularly those of the A and B series reporters, the *Slc26a5*-E1+E2 reporter was used as a control to normalize the relative intensities. In each experiment batch, same doses (1e10 gc per mouse) of AAV reporters, including the control reporter, were injected into the cochleae of neonatal mice on the same day. Tissues to be compared were collected on the same day to maintain consistency across samples. Further, images were taken using consistent parameters on the confocal microscope to ensure accuracy and comparability.

Scanning electron microscopy

After anesthetizing mice with Zoletil®50 (60 mg/kg, 0.2% Xylazine), a sequential perfusion was performed using physiological saline, followed by 4% PFA. Temporal bones were dissected post-mortem and fixed overnight at 4 °C in 2.5% glutaraldehyde. Subsequently, specimens underwent three washes with 0.01 M PBS. Decalcification of the temporal bones occurred at room temperature for 2-4 hours using 0.5 M EDTA (pH 8.0), and the organ of Corti was dissected into apical, middle, and basal regions. Samples were post-fixed for 2 hours at 4 °C with 1% osmium tetroxide, followed by immersion in 2% tannic acid for 30 minutes, repeated twice. Subsequently, specimens were dehydrated through a graded ethanol series: 30%, 50%, 70%, 90%, and 100%. After drying with a critical point dryer, samples were placed on monocrystalline silicon wafers with conductive silver, further coated with an 8 nm layer of gold using a vaccum coater, and observed using a low-voltage, high-resolution field-emission scanning electron microscope.

Auditory brainstem response test

Auditory brainstem response (ABR) signals were recorded using the Tucker-Davis Technology System III within a soundproof chamber maintained at a constant temperature of 28°C. For ABR testing, mice were anesthetized with Zoletil®50 (60 mg/kg, 0.2% xylazine), adjusting dosages based on individual weights to ensure proper anesthesia. The testing sessions were conducted at various time points as detailed in the main text. During ABR testing, subdermal electrodes were inserted separately into the test ear, brainstem, and hindlimb regions of the mice to detect hearing thresholds at 6 frequencies: 5.6 kHz, 8 kHz, 11.3 kHz, 16 kHz, 22.6 kHz, and 32 kHz. The sound intensity for each frequency ranged from 90 dB, decreasing in 5-10 dB steps to 20 dB, with the threshold defined as the lowest sound pressure level at which the ABR waveform completely disappeared. For each frequency, 512 responses were averaged, with alternating stimulus polarities. The acquired ABR response signals underwent signal processing, including amplification by a factor of 10,000, filtering within the range of 0.1-3 kHz, and presentation using a computer-based data acquisition system.

Distortion product otoacoustic emission test

Distortion product otoacoustic emission (DPOAE) testing is an auditory assessment method designed to evaluate the distortion product otoacoustic emissions originating from the cochlea. In this experimental setup, two interrelated acoustic signals (f1 and f2) are simultaneously introduced into the ear with a fixed frequency ratio. The ER10B+ probe microphone and BioSigRP software were employed for DPOAE measurements in this study. The frequency ratio of the primary tones (f1 and f2) was set at 1.2, with f2 frequencies of 5.6 kHz, 8 kHz, 11.3 kHz, 16 kHz, 22.6 kHz, and 32 kHz. The sound levels of f1 and f2 were adjusted from 80 dB SPL to 20 dB SPL in decrements of -5 dB SPL. DPOAE signals were recorded using a custom coupler placed in the external ear canal. Averaging 100 sweeps at each frequency, the DPOAE threshold was defined as the lowest sound pressure level capable of consistently eliciting a response exceeding the noise floor by 6 dB SPL. This comprehensive approach ensured accurate and reliable measurements of DPOAE across a range of frequencies, contributing valuable insights into cochlear function in the experimental subjects.

Gene therapy study

We adopt a *Slc26a5* dysfunction mouse model in this study. The full-length coding sequence of prestin (*Slc26a5* isoform1; NM_030727.5) was amplified from murine cochlear cDNA and cloned into pAAV vectors with different promoter or enhancers. After AAV package and purification as described, AAVs were administrated though round window injection (RWI) at P3. ABR and DPOAE assessments were performed at P30 to evaluate hearing function in the context of gene therapy. Scanning electron microscopy (SEM) was employed to examine the morphology and quantity of cochlear stereocilia. Immunofluorescence staining and confocal imaging were utilized to measure the expression of prestin, as well as the quantification of hair cells and ribbon synapses.

QUANTIFICATION AND STATISTICAL ANALYSIS

The data are presented as the mean ± SEM. Statistical analyses were conducted using Microsoft Excel and GraphPad Prism 8.0 software. Two-tailed, unpaired Student's *t*-tests were employed for all analyses. Error bars and *n* values are defined in the corresponding figures and legends. Statistical significance is denoted in the figures as follows: NS, not significant; *$P < 0.05$; **$P < 0.01$; ***$P < 0.001$, [#] $P < 0.05$; [##] $P < 0.01$; [###] $P < 0.001$.

Supplemental information

Deciphering enhancers of hearing loss genes

for efficient and targeted gene therapy

of hereditary deafness

Simeng Zhao, Qiuxiang Yang, Zehua Yu, Cenfeng Chu, Shengqi Dai, Hongli Li, Min Diao, Lingyue Feng, Junzi Ke, Yilin Xue, Qifang Zhou, Yan Liu, Hanhui Ma, Chao-Po Lin, Yong-Gang Yao, and Guisheng Zhong
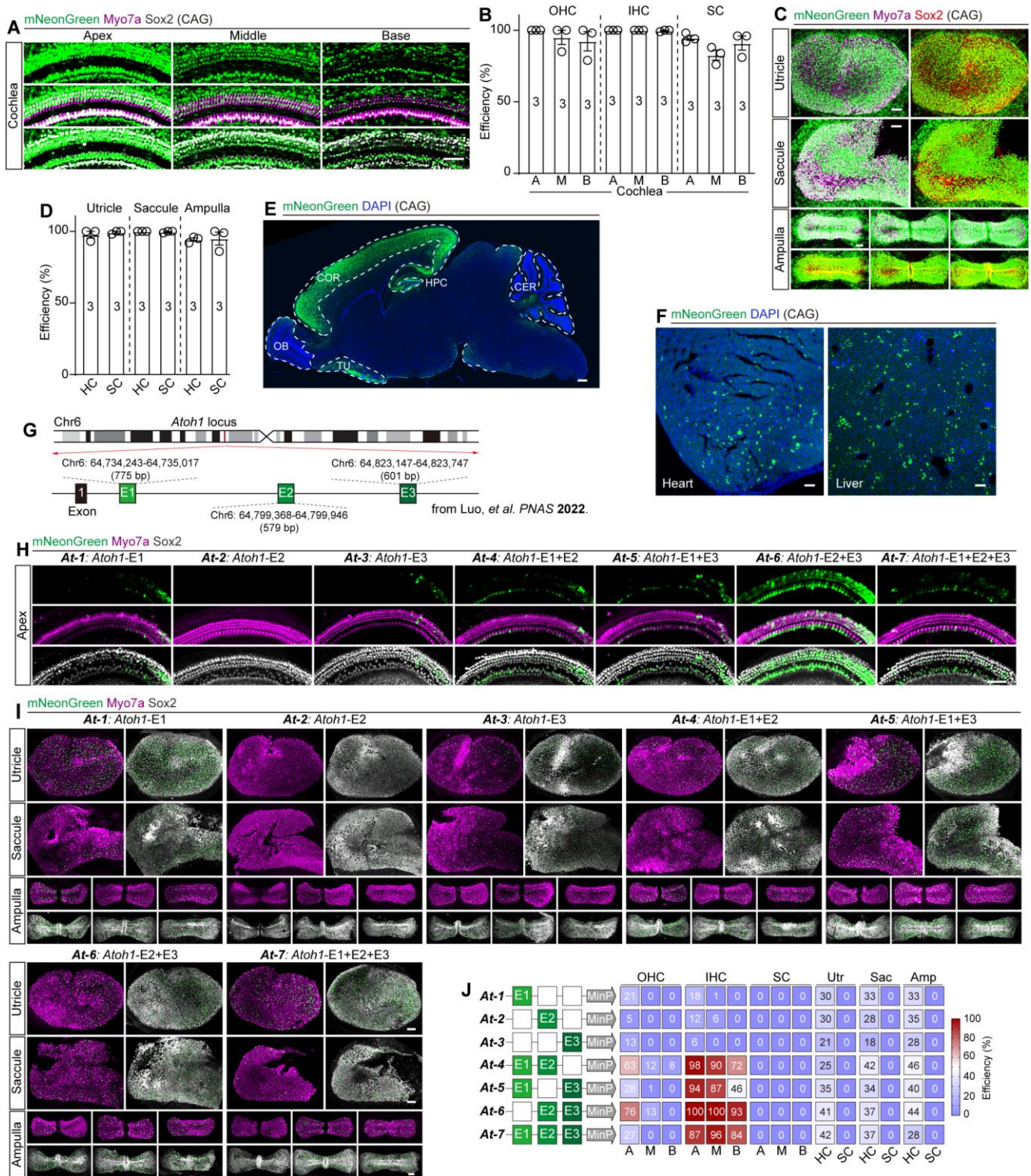
Figure S1. Establishment and validation of the ARBITER workflow-related to Figure 1.

(A) Representative fluorescence images of AAV-ie-CAG-nls-mNeonGreen infected HCs and SCs in the apical, middle, and basal regions. AAV-ie-CAG-nls-mNeonGreen was administered at the dose of 1e10 gc per mouse at P2, and samples were collected at P16 for analysis.

(B) Statistics of transduction efficiency of AAV-ie-CAG-nls-mNeonGreen in OHCs, IHCs, and SCs in different regions. *n* number in each group was labelled in the column.

(C) Transduction of vestibular cells by AAV-ie-CAG-nls-mNeonGreen.

(D) Statistics of transduction efficiency of AAV-ie-CAG-nls-mNeonGreen in vestibular HCs and SCs. *n* number in each group was labelled in the column.

(E) Representative image of AAV-ie-CAG-nls-mNeonGreen infected brain. COR, cortex. HPC, hippocampus. OB, olfactory bulb. TU, tuber cinereum. CER, cerebellum.

(F) Representative image of AAV-ie-CAG-nls-mNeonGreen infected heart and liver.

(G) Schematic illustration of the locations of *Atoh1* enhancers.

(H) Representative fluorescence images of infected cells in the apical region by the indicated synthetic enhancers. AAV reporters were delivered at P1 at the dose of 2e10 gc per mouse and collected samples at P7.

(I) Representative fluorescence images of infected vestibular cells by the indicated synthetic enhancers.

(J) Transduction efficiencies of indicated elements on targeting cochlear and vestibular cells. Average transduction efficiencies from three independent experiments in each group were presented as a heatmap and labelled in the matrix. Scale bar, 50 μm.
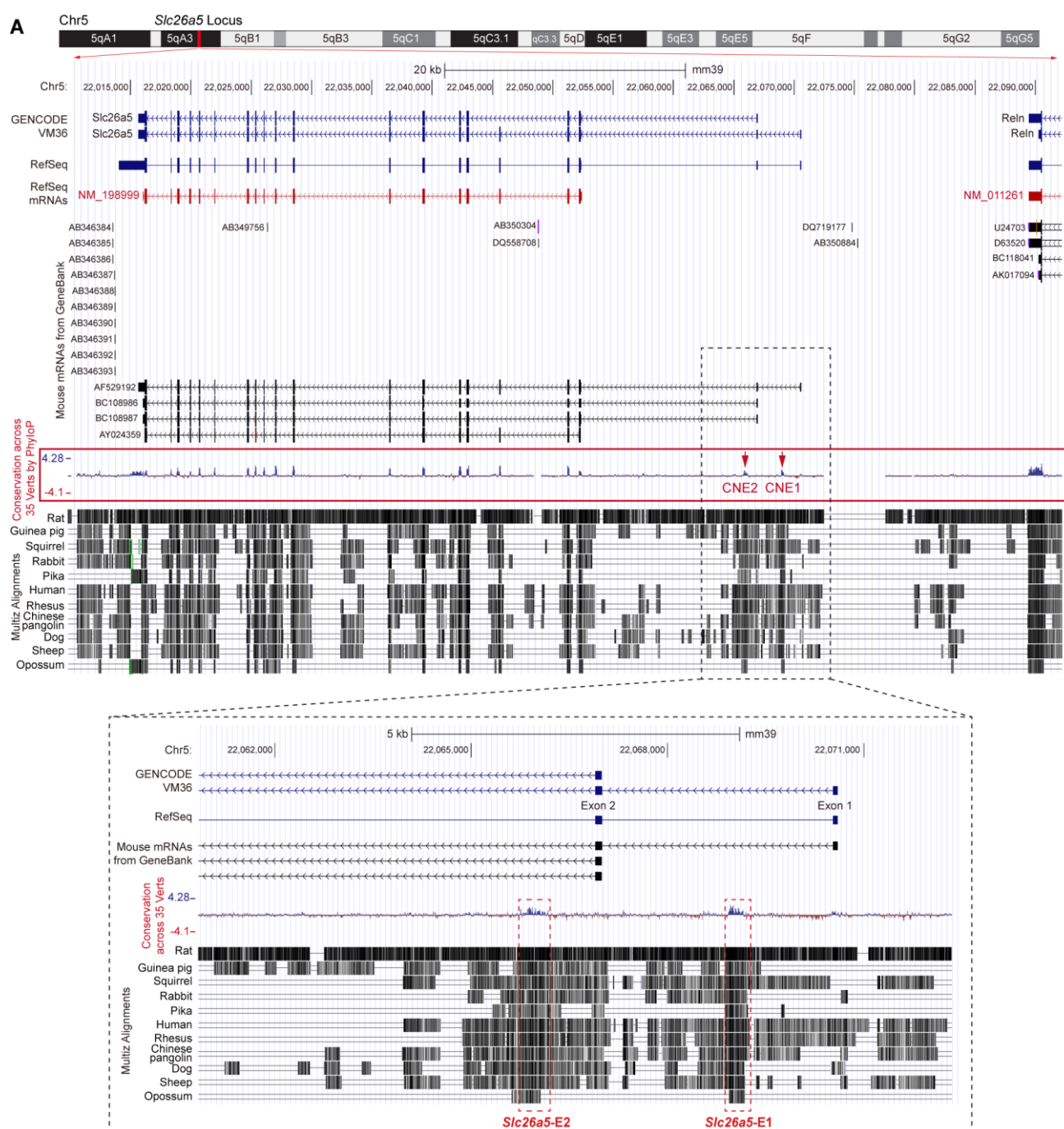
Figure S2. **Definition and criteria for CNE selection within the *Slc26a5* locus** -related to Figure **2**.

(A) An illustration depicting the definition and selection process for CNEs. CNEs were analyzed and selected using the UCSC genome browser (http://genome.ucsc.edu), which provides a visual display of various dataset tracks, such as localization, GENCODE, reference sequences, mRNAs from Genebank, Phylop score, and Multiz Alignments, etc. The Phylop scores, measuring evolutionary conservation across multiple species (highlighted in red square) were employed to select the CNEs of genes of interest. Additionally, the Multiz Alignments track presents a concise view of sequences from different species. In this study, we defined the CNEs as those longer than 100 bp with a Phylop score surpassing 1.0. In the case of *Slc26a5*, the genome browser displayed two non-coding sequences with

high Phylop scores (as seen in the zoom-in view) within the gene locus. We selected these two sequences as the candidate elements, designated as *Slc26a5*-E1 and *Slc26a5*-E2.
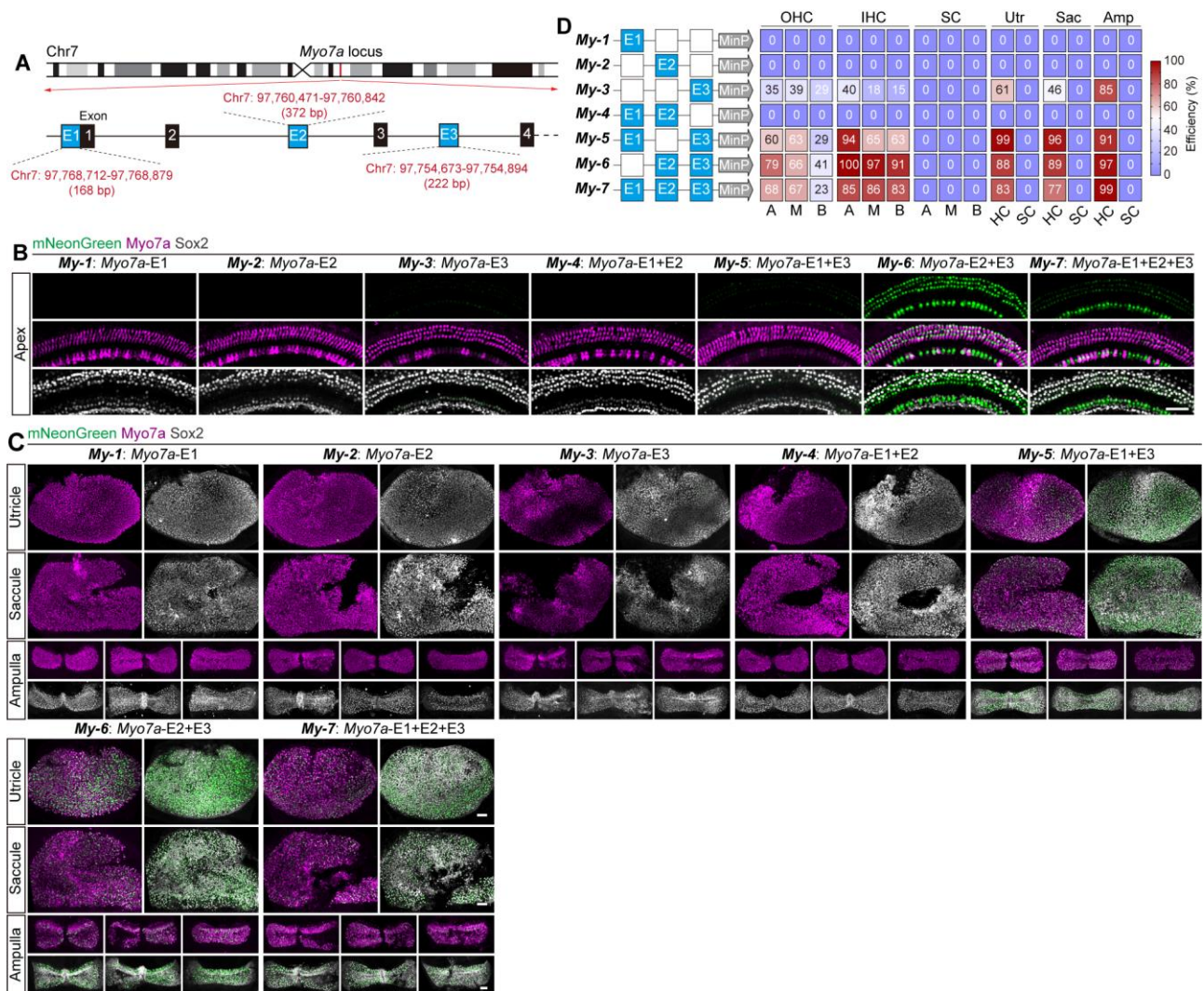
Figure S3. **Identification of transcriptional enhancers of *Myo7a*-related to Figure 2**.

(A) Schematic illustration of the localization of selected elements attributed to the *Myo7a* gene. Three CNEs, namely *Myo7a*-E1 to E3 were selected.

(B) Representative fluorescence images of infected cochlear cells in the apical region by the enhancers derived from *Myo7a*. Reporters were administered at P2 at the dose of 1e10 gc per mouse and samples were collected at P16.

(C) Representative fluorescence images of infected vestibular cells by the indicated synthetic enhancers derived from *Myo7a*.

(D) Quantification of the transduction efficiencies of the *Myo7a*-derived enhancers in cochlear and vestibular cells. Scale bar, 50 μm.

Figure S4. **Phenotype characterization of *Slc26a5*-E1 knockout mice-related to Figure 3**.

(A-C) Representative cochlear immunostaining of prestin in the apical, middle, and basal regions of wild-type, heterozygous *Slc26a5*-E1 knockout, and homozygous *Slc26a5*-E1 knockout mice at P6 (A), P16 (B), and P30 (C). Scale bar, 50 μm.

(D) Relative prestin intensities in the apical, middle, and basal regions of indicated mice at P6, P16, and P30. Intensities were normalized to the apical prestin intensities of wild-type mice at indicated time. *n* number in each group was labelled in the column.

(E) Representative SEM images of OHCs in the apical, middle, and basal regions from indicated mice at P30. Scale bar, 2.5 μm.

(F and G) ABR (F) and DPOAE (G) thresholds across frequencies of indicated mice at indicated time. *n* number in each group was labelled in the legend. ABR, auditory brainstem response. DPOAE, distortion product otoacoustic emission. Data were shown as mean ± sem, * $p < 0.05$, ** $p < 0.01$, *** $p < 0.001$, NS, no significance. Group differences were analyzed by unpaired two-tailed t test. For F

and G, differences between wild-type and heterozygous *Slc26a5*-E1 knockout mice were labelled in green, differences between wild-type and homozygous *Slc26a5*-E1 knockout mice were labelled in orange.
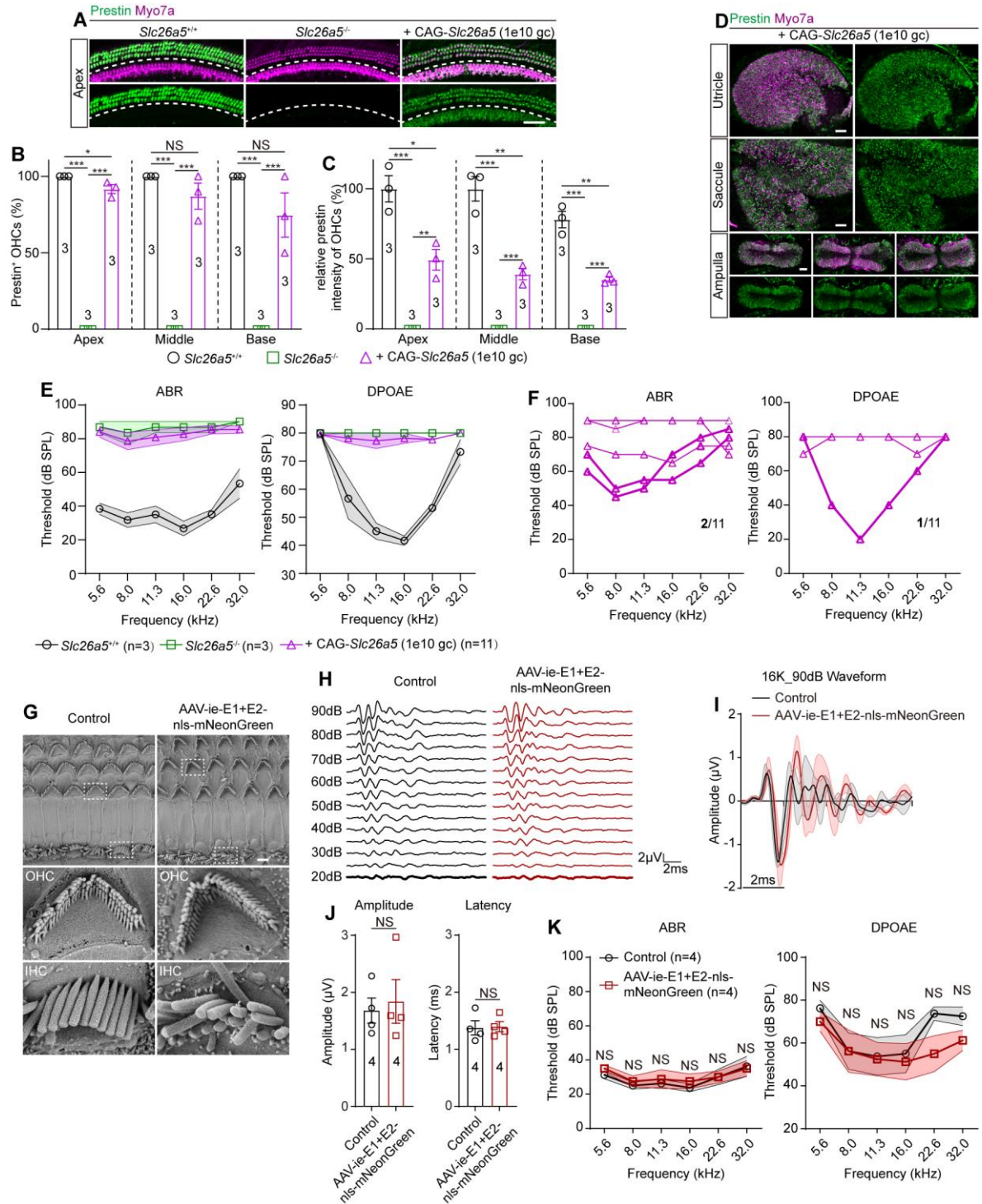
Figure S5. **Evaluation of CAG promoter based gene therapy in *Slc26a5* knockout mice and safety evaluation of *Slc26a5*-E1+E2 enhancer-related to Figure 4**.

(A) Representative cochlear immunostaining of prestin and Myo7a in the apical regions of mice from indicated group. AAV vectors were administered to the cochleae of *Slc26a5*^{-/-} mice at P3, and samples were collected at P30. Scale bar, 50 μm.

(B and C) Statistics of prestin[+] OHC populations (B) and relative prestin intensities of OHCs (C) in the apical, middle, and basal regions. Prestin intensities were normalized to apical OHCs of WT mice.

n number in each group was labelled in the column.

(D) Representative prestin staining in vestibular HCs after gene therapy using CAG promoter. Scale bar, 50 μm.

(E) Comparisons of ABR and DPOAE thresholds across frequencies between mice from indicated group, *n* numbers in each group were labelled in the legend.

(F) Individual ABR and DPOAE thresholds across frequencies of gene therapy rescued mice from indicated groups. The bold line indicated the thresholds of mice with significant functional restoration after gene therapy. The denominator indicated the number in each group and the numerator indicated the number of mice with significant functional restoration.

(G) Representative SEM images of HCs of cochleae whole mount prepared from control and AAV-ie-E1+E2-nls-mNeonGreen delivered mice. scale bar, 2.5 μm.

(H) Representative ABR waveforms at 16 kHz across all sound pressure levels, the bold line indicated the ABR thresholds.

(I) Plot of ABR waveforms evoked at 16 kHz by 90 dB SPL from control and AAV-ie-E1+E2-nls-mNeonGreen delivered mice.

(J) Statistics of peak amplitudes and latencies of ABR wave 1 evoked at 16 kHz by 90 dB SPL from control and AAV-ie-E1+E2-nls-mNeonGreen delivered mice. $n = 4$ in each group.

(K) Comparisons of ABR and DPOAE thresholds across frequencies between control and AAV-ie-E1+E2-nls-mNeonGreen delivered mice. $n = 4$ in each group. Data were shown as mean ± sem. * $p < 0.05$, ** $p < 0.01$, *** $p < 0.001$, NS, no significance. Group differences were analyzed by unpaired two-tailed t test.
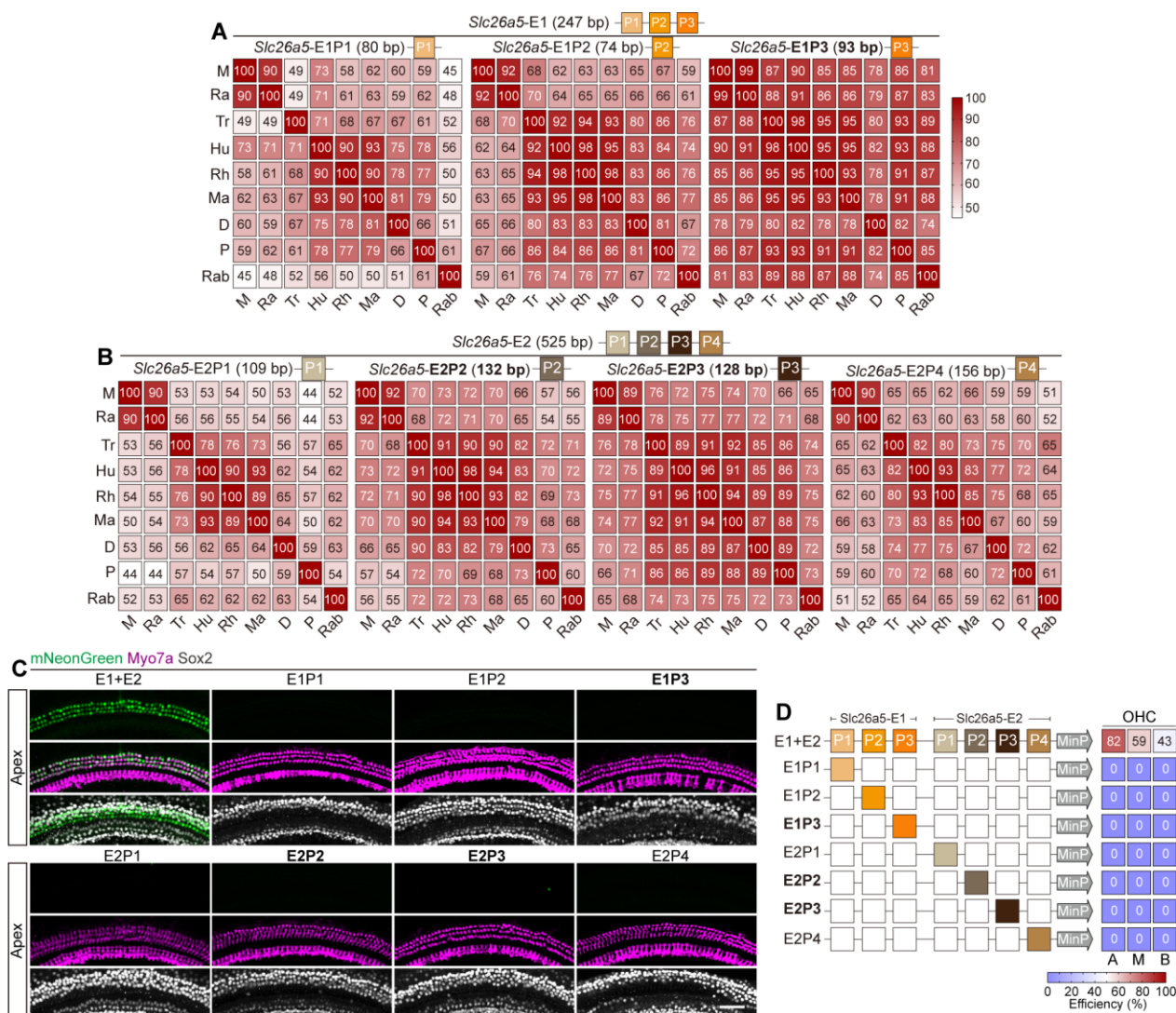
Figure S6. *In vivo* transduction evaluation of split elements derived from *Slc26a5*-E1 and E2 enhancers-related to Figure 5.

(A and B) Sequence alignment identity of split E1 (A) and E2 (B) elements across species. The abbreviations are same to those in Figure 2. E1 was split into three parts to generate E1P1, E1P2, and E1P3, respectively based on the conservation. E2 was split into four parts to generate E2P1, E2P2, E2P3, and E2P4 respectively. Identity across species was labelled in the matrix.

(C) Representative fluorescence images of infected OHCs in the apical region by the indicated split modules, the full-length E1+E2 enhancer was used as control. Reporters were delivered at P2 at the dose of 1e10 gc per mouse and samples were collected at P16 for analysis. Scale bar, 50 μm.

(D) Statistics of transduction efficiencies of indicated modules on targeting OHCs. Average transduction efficiencies from three independent experiments in each group were presented.
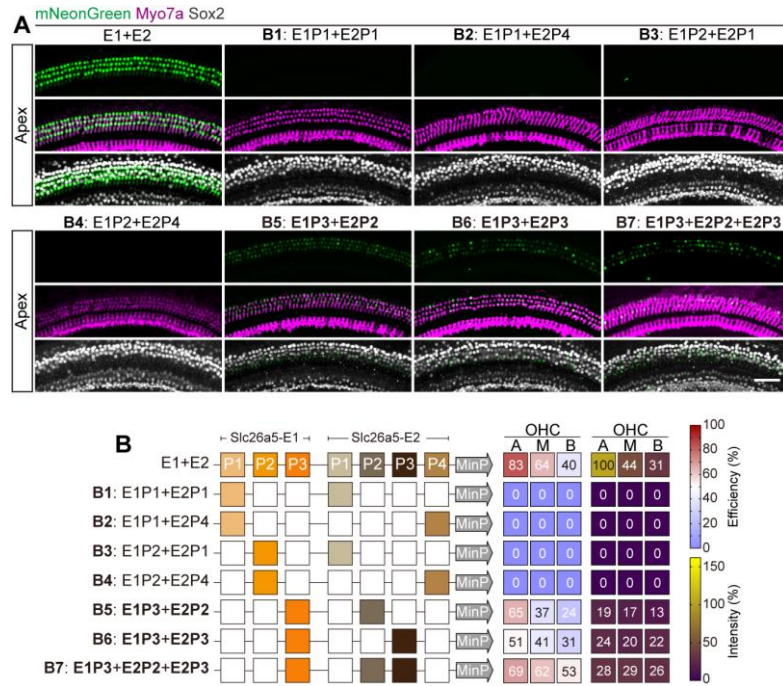
Figure S7. **Key module combinations are sufficient to induce OHC-specific gene expression-related to Figure 6**.

(A) Representative fluorescence images of infected OHCs in the apical region by the indicated enhancers, with the full-length E1+E2 enhancer as a control. Reporters were delivered at P2 at the dose of 1e10 gc per mouse and samples were collected at P16 for analysis. Scale bar, 50 μm.

(B) Statistics of transduction efficiencies and intensities of indicated modules on targeting OHCs. Average transduction efficiencies and intensities from three independent experiments in each group were presented.

Table S1. Primers used for genotyping, related to STAR Methods

Primer	Sequences (5' to 3')	Function	Product
Slc26a5−E1 KO-F1	CCACAATGAATTGCAGCCCTG	*Slc26a5*-E1 knockout mice genotyping	339 bp for wild type mice and no amplicon for *Slc26a5*-E1$^{-/-}$ mice
Slc26a5−E1 KO-R1	TGGATTGAGCC GATCCTTTTG		
Slc26a5−E1 KO-F2	GGCTTGTGATACCGCTAGAACTAGA	*Slc26a5*-E1 knockout mice genotyping	1291 bp for wildtype mice and 651 bp for *Slc26a5*-E1$^{-/-}$ mice
Slc26a5−E1 KO-R2	GTATTTGGGACGTATGAG CAGGTG		
Slc26a5−E2 KO-F1	TGGCTCTCAACCACGTATGGAGAT	*Slc26a5*-E1+E2 double knockout mice genotyping	594 bp for wildtype mice and no amplicon for *Slc26a5*-E1$^{-/-}$E2$^{-/-}$ mice
Slc26a5−E2 KO-R1	CGTCGAGGCGAGAGATCATCTT		
Slc26a5−E2 KO-F2	GTGTGTAACAGTAGGACAGTACAGGACC	*Slc26a5*-E1+E2 double knockout mice genotyping	1313 bp for wild type mice and 581 bp for *Slc26a5*-E1$^{-/-}$E2$^{-/-}$ mice
Slc26a5−E2 KO-R2	AGTTGTCTTTAATGGTGGCTGGA		
Slc26a5 KO-F1	CCACCACGTTTAGTAGCATC	*Slc26a5* knockout mice genotyping	Amplicon (402 bp) for sanger sequencing
Slc26a5 KO-R1	ACTGTGATGAACATGAGCCA		